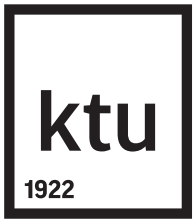


KAUNAS UNIVERSITY OF TECHNOLOGY
FACULTY OF ELECTRICAL AND ELECTRONICS ENGINEERING

**Dainius Stankevičius**

# PHOTOPLETHYSMOGRAPHY-BASED SYSTEM FOR ATRIAL FIBRILLATION DETECTION DURING HEMODIALYSIS

Master's Thesis

**Supervisor**
Prof. Dr. Vaidotas Marozas

**KAUNAS, 2016**

KAUNAS UNIVERSITY OF TECHNOLOGY
FACULTY OF ELECTRICAL AND ELECTRONICS ENGINEERING
DEPARTMENT OF ELECTRONICS ENGINEERING

# PHOTOPLETHYSMOGRAPHY-BASED SYSTEM FOR ATRIAL FIBRILLATION DETECTION DURING HEMODIALYSIS

Master's Thesis

**Biomedical Engineering (621H16001)**

**Supervisor**

(signature) Prof. Dr. Vaidotas Marozas

(date)

**Reviewer**

(signature) Prof. Dr. Linas Svilainis

(date)

**Author**

(signature) Dainius Stankevičius

(date)

**KAUNAS, 2016**


KAUNAS UNIVERSITY OF TECHNOLOGY

Faculty of Electrical and Electronics Engineering
(Faculty)

Dainius Stankevičius
(Student's name, surname)

Biomedical Engineering, 621H16001
(Title and code of study program)

„Photoplethysmography-Based Atrial Fibrillation Detection During Hemodialysis“ final project

**DECLARATION OF ACADEMIC HONESTY**

3 June 2016

Kaunas

I confirm that a final project by me, Dainius Stankevičius, on the subject „Photoplethysmography-Based Atrial Fibrillation Detection During Hemodialysis“ is written completely by myself, all provided data and research results are correct and obtained honestly. None of the parts of this thesis have been plagiarized from any printed or internet sources. All direct and indirect quotations from other resources are indicated in literature references. No monetary amounts not provided by law have been paid to anyone for this thesis. I understand that in case of a resurfaced fact of dishonesty, penalties will be applied according to the procedure effective at Kaunas University of Technology.

*(name and surname filled in by hand)* *(signature)*

Stankevicius, D. Photoplethysmography-Based System for Atrial Fibrillation Detection During Hemodialysis. Final project of biomedical engineering master's qualification degree / supervisor prof. dr. Vaidotas Marozas; Kaunas University of Technology, Faculty of Electrical and Electronics Engineering, department of Electronics Engineering.

Kaunas, 2016. 60 p.

## SUMMARY

Atrial fibrillation is a relevant problem among patients undergoing hemodialysis. A study based on the health insurance records showed that the risk of developing atrial fibrillation for hemodialysis patients is 10 times higher when compared to the general population. A more recent study, based on the data from implantable cardiac monitors, showed that more than half of the participating hemodialysis patients experienced atrial fibrillation. Although electrocardiography is a reliable way to detect atrial fibrillation, it is too encumbering for the monitoring of hemodialysis patients. In this work, we propose an unobtrusive system for atrial fibrillation detection. The system consists of a wearable device and integrated algorithm for real-time atrial fibrillation detection using solely the photoplethysmogram. The algorithm is based on the heart rate irregularity and consists of low-pass filter for high-frequency noise removal, adaptive filter for baseline removal, slope sum function and adaptive threshold for peak detection, low-complexity atrial fibrillation detector for decision making, and mean-crossing rate based measure for signal quality assessment. A set of 2200, 1-minute-long photoplethysmogram and electriocardiogram signals has been collected from the public Physionet MIMIC database. The algorithm was implemented in Matlab environment and in embedded system. When testing the performance of the algorithm with the collected set of noise-free signals, the sensitivity of 0.99 and the perfect specificity of 1 were obtained. The embedded system was tested with one representative signal and no differences were observed. The performance of the proposed low-quality-signal detector showed a sensitivity of 0.99 and a specificity of 0.90 for a distinction between noise-free photoplethysmogram and photoplethysmogram contaminated with added noise during both - atrial fibrillation and normal rhythms.

*Keywords*:
photoplethysmography; atrial fibrillation; hemodialysis; wearable device; photoplethysmogram quality assessment; embedded system; photoplethysmogram signal processing; unobtrusive system.

Stankevičius, D. Fotopletizmografija pagrįsta sistema prieširdžių virpėjimui atpažinti hemodializės procedūrų metu. Biomedicininės inžinerijos magistro kvalifikacinio laipsnio baigiamasis projektas / vadovas prof. dr. Vaidotas Marozas; Kauno technologijos universitetas, Elektros ir elektronikos fakultetas, Elektronikos inžinerijos katedra.

Kaunas, 2016. 60 psl.

## SANTRAUKA

Prieširdžių virpėjimas yra svarbi problema hemodializės pacientų grupėje. Sveikatos draudimo duomenimis pagrįstas tyrimas parodė, kad prieširdžių virpėjimo išsivystimo rizika hemodializės pacientams yra 10 kartų didesnė lyginant su bendra populiacija. 2015 metais atliktas tyrimas, pagrįstas duomenimis iš implantuojamų širdies monitorių, parodė, kad daugiau kaip pusei iš stebėtų pacientų išsivystė prieširdžių virpėjimas. Nors elektrokardiografija yra patikimas būdas prieširdžių virpėjimui aptikti, tačiau tai nėra pakankamai patogus metodas hemodializuojamiems pacientams stebėti. Šiame darbe pristatome pacientui netrukdančią sistemą prieširdžių virpėjimui aptikti. Sistemą sudaro dėvimas įrenginys ir mažai matematinių operacijų reikalaujantis realaus laiko algoritmas prieširdžių virpėjimui aptikti naudojant tik fotopletizmografinį signalą. Algoritmas remiasi širdies ritmo nereguliarumu ir susidaro iš: žemų dažnių filtro aukšto dažnio triukšmui pašalinti, adaptyvaus filtro bazinei linijai pašalinti, impulsų fronto sumos funkcijos ir adaptyvaus slenksčio pikams aptikti, mažo kompleksiškumo prieširdžių virpėjimo detektoriaus sprendimui priimti, vidurkio kirtimo dažniu pagrįsto algoritmo signalo kokybei vertinti. Naudojantis atviros Physionet MIMIC duomenų bazės įrašais buvo sudarytas signalų rinkinys iš 2200 fotopletizmografinių ir elektrokardiografinių signalų, kurių kiekvienas yra vienos minutės ilgio. Algoritmas buvo įgyvendintas Matlab aplinkoje ir įterptinėje sistemoje. Testuojant algoritmą su surinktais betriukšmiais signalais nustatytas jautrumas lygus 0.99 ir specifiškumas lygus 1. Įterptinė sistema buvo išbandyta su vienu reprentatyviu signalu ir jokių skirtumų nepastebėta. Algoritmo signalo kokybei vertinti rezultatai parodė jautrumą lygų 0.99 ir specifiškumą lygų 0.90 klasifikavimui tarp betriukšmių signalų ir signalų su pridėtiniu triukšmu.

*Reikšminiai žodžiai:*

fotopletizmografija; prieširdžių virpėjimas; hemodializė; dėvimas įrenginys; fotopletizmogramos kokybės įvertinimas; įterptinė sistema; fotopletizmografinių signalų apdorojimas; pacientui netrukdanti sistema.

## ACKNOWLEDGMENTS

I would like to express my gratitude to my supervisor Dr. Vaidotas Marozas for the useful remarks, engagement and continuous support through this master's thesis.

I would also like to thank my colleagues Dr. Andrius Petrėnas and Andrius Sološenko for debates, editorial assistance, and also for cooperation in preparing related conference publications. I must thank Andrius Sološenko additionally, for the enormous work accomplished while manually collecting the signal set, which was used in this work.

Finally, I would like to note that this work was partially supported by the project CARRE, funded by the European Commission under the grant No. FP7-ICT-611140, and the project AFAMI, funded by the Research Council of Lithuania under the grant No. MIP088.

# Contents

**Terms and Definitions**

ECG - electrocardiogam

PPG - photoplethysmogram

SSF - slope sum function

AF - atrial fibrillation

LED - light-emitting diode

LA - left atrium

RA - right atrium

LV - left ventricle

RV - right ventricle

QRS complex - a complex of Q, R and S peaks in electrocardiogram

bpm - beats per minute

LMS - Least Mean Squares

SNR - signal-to-noise ratio

# Introduction

End-stage renal disease is considered as an important public health problem. The only effective treatment is a renal replacement therapy, such as hemodialysis or kidney transplantation. Hemodialysis is a procedure during which a cardiovascular system of a patient is connected to an external artificial kidney machine to clean blood from toxins and excess fluids. This procedure usually takes place 3-4 times a week. The hemodialysis causes an overload on the cardiovascular system, which is related to changes in fluid and electrolyte balance, resulting in arrhythmias, such as atrial fibrillation (AF) [1, 2].

AF is a superventricular arrythmia by which a chaotic and uncontrollable activation and contraction of atria occur [3]. AF is the most common arrhythmia in clinical practice, affecting more than 33 million people around the world [4]. Even short episodes of AF are related to increased risk of health issues, such as ischemic stroke or heart failure [5]. The risk of developing AF for general population increases due to an old age. However, the risk of developing AF highly increases for patients undergoing hemodialysis due to the already mentioned factors [6]. Given that the procedure of hemodialysis should be stopped if AF occurs, timely detection of this arrhythmia is vitally important.

Although electrocardiography is a reliable way to detect AF, this technique is not convenient enough for hemodialysis patients. Most of the patients in hemodialysis are chronically sick and unwilling to encumber their routine procedure. In addition, attachment of electrodes for electrocardiography is time-consuming and requires additional material resources. Considering these points, a more convenient way to detect AF during hemodialysis is highly desirable.

To overcome this problem, we propose an unobtrusive approach, based on photoplethysmography. Photoplethysmography is an optical method for measuring blood flow in tissue near the surface of the skin. Each cardiac cycle appears as a peak in a photoplethysmogram (PPG). A conventional PPG is obtained by illuminating the skin with light-emitting diode (LED) and measuring the reflected (or transmitted) light with photodiode. Therefore, only one small contact site is required. The PPG device can be placed on a convenient site of the body, such as finger, wrist, upper arm, forehead, etc. While electrocardiography has been used for AF detection for many years, the intersection of photoplethysmography and AF is quite new. To the best of our knowledge, there has been only one research dedicated to the unobtrusive AF detection using PPG [7]. However, the latter method, involving a camera of a smartphone, is suitable only for intermittent monitoring, while we propose a long-term monitoring approach.

**The aim** of this work is to develop an unobtrusive system for real-time atrial fibrillation detection during hemodialysis. **The objectives** are the following:

1. To develop an algorithm for atrial fibrillation detection, which would be based solely on the processing of photoplethysmogram and would not require high computational resources.
2. To develop a detector of the low-quality-photoplethysmogram.
3. To implement the algorithm in a low-power wearable embedded system.
4. To investigate the performance of the algorithm with a set of photoplethysmogram signals containing episodes of atrial fibrillation.

# 1. Background

This chapter presents the background information regarding the physiological information, relevance of the problem and related methodology.

## 1.1. Clinical Background

This section presents the physiological background information, relevance of AF, chronic kidney disease, and the relation between the diseases.

### 1.1.1 Heart and Kidneys

The heart is a muscular organ which pumps blood through the body via the blood vessels. The main function of the blood circulation is to provide the oxygen and nutrients to the body and remove metabolic wastes. In humans, the heart is divided into four chambers (see Fig. 1.1) left and right atria (LA and RA), which receive the blood, and left and right ventricles (LV and RV), which pump the blood out. The blood flows in one way through the heart because of the heart valves. Blood, which is low in oxygen, first enters the right atrium and then the right ventricle. From there the blood is pumped to the lungs where it receives oxygen and gives away carbon dioxide, and returns back to the left atrium. The oxygenated blood passes through the left ventricle and is pumped out to the systemic circulation through the aorta. In the systemic circulation the oxygen is used and the deoxigenated blood returns back again to right atrium.

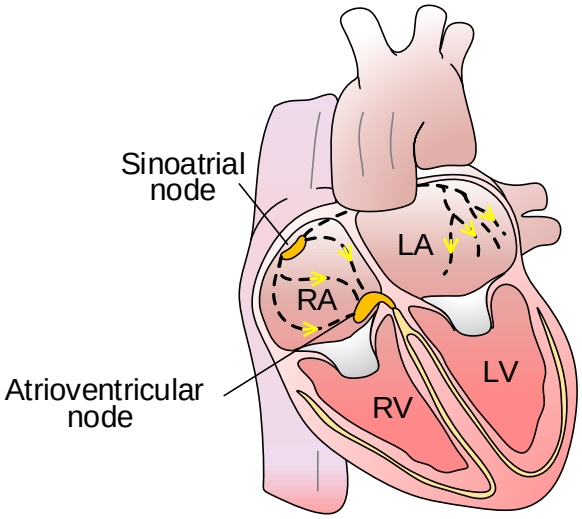


Figure 1.1: The structure of the normal heart: LA - left atrium, RA - right atrium, LV - left ventricle, RV - right ventricle; adapted from [8]

The kidneys are bean-shaped organs responsible for regulation of the balance of elec-

trolytes in the blood. The main function of the kidneys is to remove the waste products of metabolism from the body. They act as a natural filter of the blood diverting the wastes to the bladder and producing urine. They are also responsible for the re-absorption of water, glucose, amino acids, and the production of several hormones. The kidneys receive blood via the renal arteries, dismiss blood to renal veins, and excretes urine in to the bladder.

### 1.1.2 Electrocardiography and Photoplethysmography

Electrocardiography is a method for recording the electrical activity of the heart using electrodes placed on the skin [9]. The electrodes pick up small voltage changes on the skin originating from the electrical depolarization of the heart. The depolarization refers to a sudden change of electrical charge of a cell. The voltage changes over time are called electrocardiogram (ECG) signal. Sinoatrial node (see Fig. 1.1) is a natural pacemaker responsible for the initiation of the heart beat and the overall heart rate, which is between 60 and 100 bpm under resting condition. The initial electric impulse forces atria to contract and to push blood to ventricles. Then, the impulse reaches the atrioventricular node which forces the ventricles to contract and push blood out of the heart. Electrocardiography allows to observe this activity on the surface of the skin. Normally, ECG starts with P wave (see Fig. 1.2), which indicates atrial depolarization. The a QRS complex follows, which indicates ventricular depolarization. The last T wave represents ventricular repolarization.

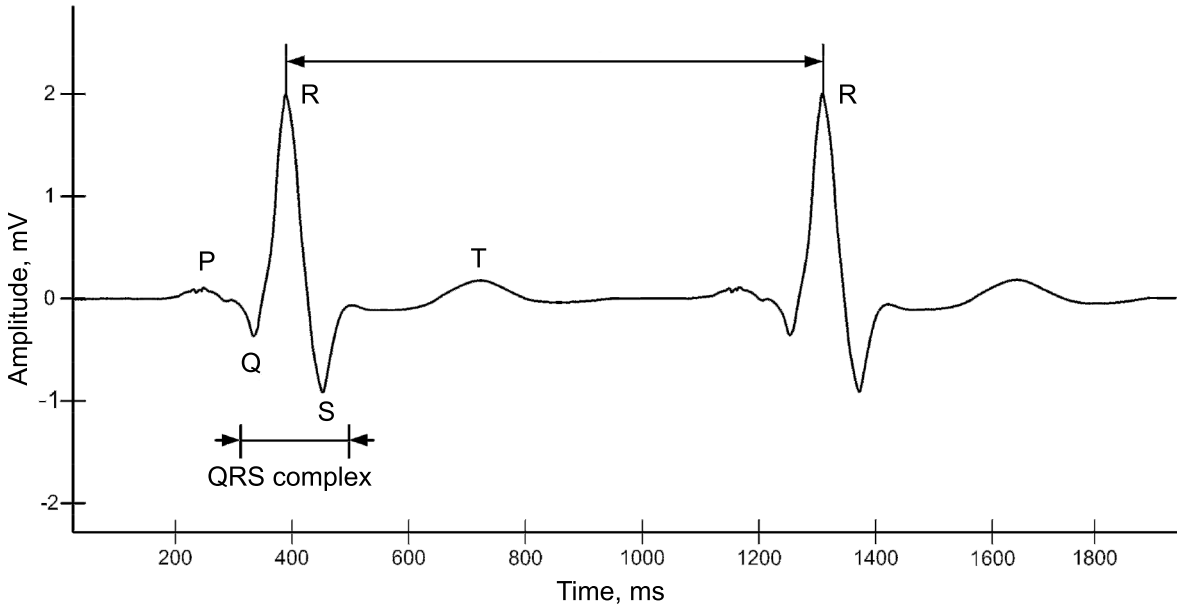


Figure 1.2: ECG morphology, adapted from [10]

Photoplethysmography is an optical method for a volumetric measurement of any organ [11]. A conventional PPG is obtained by measuring blood perfusion to the skin and surrounding tissue. During each cardiac cycle blood is pumped to the periphery and a pressure

pulse wave is formed. The change of volume caused by this pulse wave is detected by illuminating the skin with LED and measuring the amount of transmitted or reflected light with photodiode. The golden standard of PPG is the one obtained with finger pulsoximeter working in transmitted light mode. The main feature of PPG is very low alternating component when compared to baseline component (see Fig. 1.3). This phenomena occurs due to high amount of tissue, which do not indicate blood pulsation. This is also responsible for high susceptibility of PPG to motion artefacts, since even a slight deformation of tissues makes a bigger contribution to the signal than the alternating PPG component.

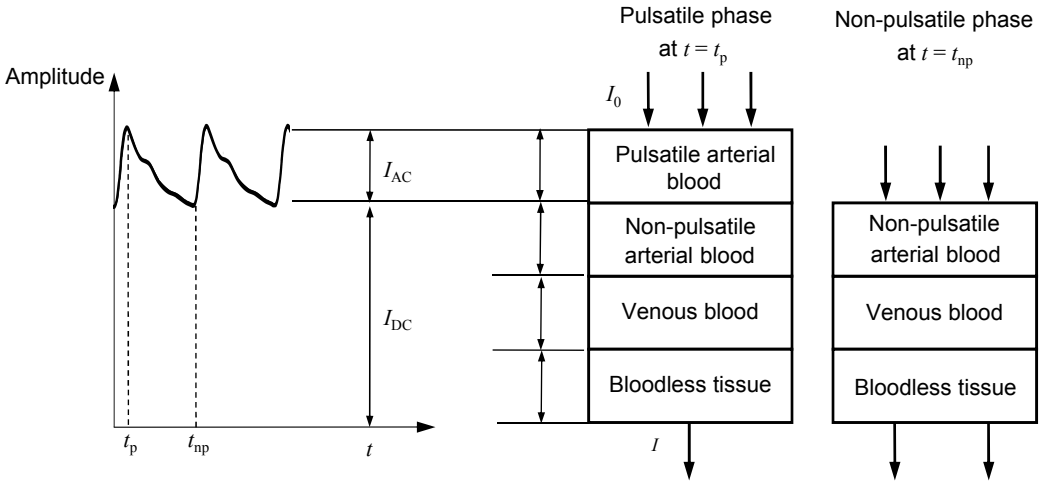


Figure 1.3: Components of the PPG signal, adapted from [11]

Each cardiac cycle appears as a peak in PPG. In a typical waveform of PPG (see Fig. 1.4), the systolic impulse represents ventricular contraction, dicrotic notch represents the relaxation of ventricles, and the diastolic impulse forms as an reflection from capilaries. The exact shape of PPG varies for each subject and for location of the measurement. While both - ECG and PPG represent the cardiac activity, it is important to note the distinction: ECG represents the electrical activity of the heart, while PPG represents mechanical activity of the cardiovascular system.

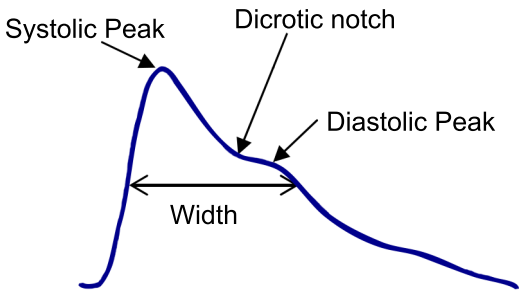


Figure 1.4: Morphology of typical PPG signal, adapted from [12]

### 1.1.3 Atrial Fibrillation

Normally, the contraction of atria is initiated by the sinoatrial node - the natural pacemaker of the heart. However, during AF, the contraction of atria is initiated chaotically by the electrical activity of localized sources in the atria itself (see Fig. 1.5) [9]. The rate of atria contraction during AF reaches up to 400-600 bpm. Some of electrical impulses pass through the atrioventricular node and causes the contraction of ventricles. Therefore, the heart rate during AF is elevated, highly irregular, and the ejected blood volume is decreased [13]. The visual distinction between AF and normal rhythm is clear in both - ECG and PPG (see Fig. 1.6).

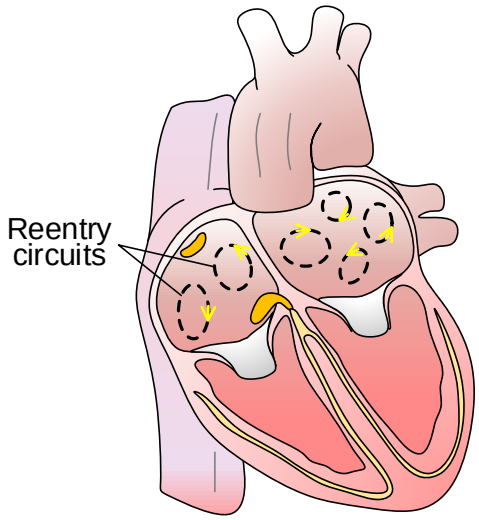


Figure 1.5: The electrical activity of the heart during AF; adapted from [8]

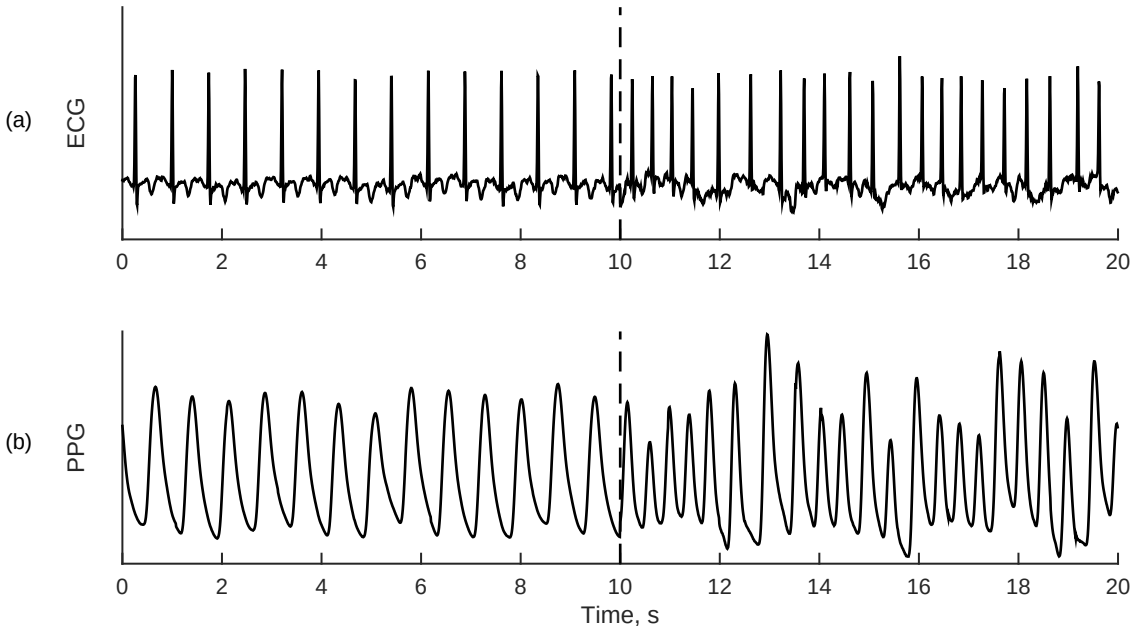


Figure 1.6: Synchronously recorded ECG (a) and PPG (b) during normal rhythm (left) and AF (right)

There are various symptoms related to AF, however up to 80 % of the cases are asymptomatic - without any noticeable symptoms [14, 15, 16, 17]. According to *European Society of Cardiology*, five types of AF are distinguished [18]:

- first diagnosed AF - irrespective of the duration or severity;
- paroxysmal AF - self-terminating, usually within 48 hours;
- persistent AF - an episode lasts longer than 7 days or requires termination by medical means;
- long-standing persistent AF - has lasted for more than 1 year and it is decided to adopt medical means for rhythm control;
- permanent AF - the rhythm control interventions are not pursued anymore.

AF is the most common arrhythmia affecting more than 33 milion people in the world [18]. It is estimated that the real percentage of people with AF might reach 2% of the population due to not diagnosed asymptomatic AF [4]. The risk of developing AF depends significantly on the age: in the age group bellow 55 years the prevalence reaches only 1.7 %, while in the age group above 84 years the prevalence reaches even 17 % [4].

AF is not a life-threatening cardiac arrhythmia by itself, but it is related to several comorbidities [19]:

- ischemic stroke (up to 51 % of the patients are also diagnosed with AF);
- heart failure (56 % of the patients are also diagnosed with AF);
- myocardial infarction (23 % of the patients after infarction are diagnosed with AF);
- high blood pressure (70 % of the patients develop AF);
- kidney diseases (up to 15 % of the patients develop AF);
- sleep apnea (50 % of the patients are diagnosed with AF).

The most important commorbidity is an ischemic stroke, which occurs when the blood flow to the brains is blocked. Up to one third of ischemic strokes occur due to trombs most of which are related to AF [20], therefore AF could be related to 15-18 % of total cases of stroke [21]. The presence of AF increases the risk of stroke up to 5 times.

The three main objectives regarding the treatment of AF [3] are:

- to prevent the formation of trombs;
- to control the rate of the ventricular contractions;
- to revert back to the normal rhythm;

Mostly, pharmaceuticals-based treatment is applied for AF patients [14]. Anticoagulant medication is used to prevent the formation of trombs. Additional medication is used to control the rate of ventricular contractions by affecting specifically the atrioventricular node. Electrical cardioversion, catheter ablation, and cardiac stimulation are non pharmaceuticals-

based treatment methods, which are applied up to 10 % of the patients [14].

### 1.1.4 Kidney Failure and Hemodialysis

The main function of kidneys is to remove excess fluids, minerals and waste from the body. When a person is diagnosed with end-stage renal disease, it means that the kidneys do not function in a normal way and a treatment to replace the kidney function is needed. There are three types of such treatment: hemodialysis, peritonial dialysis, and kidney transplantation.

Hemodialysis is the most common method used to treat advanced and permanent kidney failure, as described by the *National Institute of Diabetes and Digestive and Kidney Diseases* [22]. The purpose of hemodialysis is to filter the blood. Apart from the waste, excess water and salt, which are being removed during hemodialysis, it also helps to control blood pressure and the quantity of minerals (potassium, sodium, calcium, etc.). Blood is filtered by connecting the cardiovascular system of a patient to the special filter, called dialyser. Hemodialysis usually takes place 3 times per week, and one procedure lasts 3-5 hours. During the procedure the patients can read, write, speak, sleep, watch television, etc.

### 1.1.5 Relation between Hemodialysis and Atrial Fibrillation

Several studies have shown that hemodialysis is related to the increased risk of developing AF. One study, based on the data from over 250 000 patients, showed that almost one sixth of the patients undergoing hemodialysis are diagnosed with AF [23]. In the study, the data was taken from the *Medicare* insurance archives from year 1995 to 2007. All hemodialysis patients in the age group above 67 years were included, if they were not diagnosed with AF in the last 2 years before the hemodialysis. The aim of the study was to determine the percentage of cases of AF in the patients after the hemodialysis treatment begins. Additionally, they wanted to determine the rate of death and ischemic stroke after AF is diagnosed. The results showed that AF develops in 14.8 % of hemodialysis patients in a year in average. More importantly, the number of AF cases in hemodialysis patients increased almost threefold during the 12 years of study period (from 5.8 % of AF cases in year 1996 to 16.5 % AF cases in year 2006). The prevalence of AF in hemodialysis patients regarding the age shows similar trends to general population. According to statistics of year 2006 there were 13.2 % cases in the age group of 65-74 years, 19.2 % cases in the age group of 75-84 years; 22.5 % in the age group of over 85 years.

In the already mentioned study [23], it was shown that the rate of death in hemodialysis patients in the first year after diagnosis of AF decreased by 22 % in the 12 years of the study period. However, the absolute rate of death still remained over 50 % (59 % in year 2007).

Another study of the same research group showed that hemodialysis patients with diagnosed AF die twice as frequent as the patients without any heart arrhythmias [24].

One important question is, why the number of AF cases among the hemodialysis patients increases. There are three possible answers: the number of AF cases actually increases; AF is detected more frequently; patients with AF live longer. There comes the limitations of the study presented in [23] - the study has high specificity but low sensitivity. It is obvious that some patients with AF could have been missed due to misdiagnosis or missing health insurance records.

Another clinical study related to hemodialysis was conducted in the USA in year 2015 [25]. The aim of the research was to determine the percentage of hemodialysis patients which develop clinically important heart arrhythmias. The clinically important heart arrhythmias included ventricular tachycardia (heart rate higher than 150 bpm), bradycardia (heart rate lower than 40 bpm), asystole longer than 3 seconds, and any symptomatic event. The study included 150 hemodialysis patients. The participants received an implantable arrhythmia detector *Medtronic Reveal XT*. The trial started in January 2013 and ended in November 2015. The data was collected in 8 hospitals: 5 hospitals in the USA and 3 hospitals in India. The first results of the research were presented in conferences of *American Society of Nephrology* and *American Heart Asociation* [26], as well as in the press release by *Medtronic* [27]. The primary results confirmed that AF occurs much more frequently in hemodialysis patients than all of the other indicated arrhythmia. More than half of the participants experienced AF. The study also revealed that the risk of AF significantly increases during the first twelve hours since the beginning of the hemodialysis procedure. After twelve hours, the risk drops several-fold, but right before the next hemodialysis procedure the risk reaches its maximum again.

It is clear that the patients undergoing hemodialysis are at much higher risk of developing AF. The underlying physiological processes are not entirely known yet, but the factors which could be related to the issue include:

- periodic fluctuations of water and electrolytes during hemodialysis;
- remodeling of heart muscle;
- slow inflammation and oxidative stress.

These factors are related to the calcification of the cardiovascular system, which leads to chronic wear of the cardiovascular system and increases the stiffness of the system. We can see that AF is an important problem among the hemodialysis patients. Any means for the detection, diagnostics and treatment of AF would have a huge impact.

## 1.2. Overview of Existing Technologies

This section presents analysis of available methods for AF detection. Relevant signal databases are discussed as well.

### 1.2.1 Atrial Fibrillation Detection Using Electrocardiogram

Most of the algorithms for automatic AF detection are suited for ECG. Four main types of the algorithms could be distinguished by being based on:

- the analysis of series of RR intervals
- the absence of P waves in the ECG,
- the presence of fibrillatory f-waves,
- the combination of the previous three.

Most of the algorithms are based on the RR interval series [28] [29], while a few algorithms include the additional information of P wave and f wave [30] [31]. The latter algorithms are usually highly computationally demanding, what makes them unsuitable for implementation in embedded systems for real-time AF detection. One example of an algorithm with a low-computational-complexity based on RR interval series is presented in [32]. The algorithm requires only 8-beat sliding window and allows to tune the performance with only one design parameter.

Another algorithm published in [33] is exceptional, since it is not based on RR intervals nor the P waves. At first, the ECG signals were filtered by band-pass filter with cut-off frequencies of 0.5 Hz and 50 Hz to reduce the noise. Then, a stationary wavelet transform was applied followed by a parametrization. Two main parameters were used: peak-to-average power ratio, and logarithmic energy entropy. The support vector machine was used for the AF detection. Annotated ECG signal database and cross-validation was used for performance evaluation. The performance of the presented algorithm reached sensitivity of 0.97 and specificity of 0.97 for a clinical AF database.

### 1.2.2 Atrial Fibrillation Detection Using Photoplethysmogram

PPG allows to obtain similar heart rhythm information to the one obtained from ECG. The time interval between the two successive peaks of the PPG signal depict the time between two successive heart beats. A research based on PPG signals obtained by a smartphone camera showed that it is possible to detect AF using the PPG [7]. PPG was obtained by averaging the green channel of each frame while recording at 30 frames per second. Then peaks of the PPG were detected using filter bank with varying cut-off frequencies,

spectral heart rate calculation and non-linear filters. Statistical algorithms were applied to detect AF from peak-to-peak intervals. Three parameters were used: mean squared value of the differences between the intervals, Shenon entropy, and sample entropy. Data from annotated ECG databases was used to determine the thresholds. Real PPG signals were registered for performance evaluation. The data was collected from patients before and after electrical cardioversion at the *Massachusets University Medical Center*. The limitations of this research are related to the proposed monitoring method using a smartphone and the method for performance evaluation. First of all, monitoring via a smartphone is not suitable for long-term usage. While the authors indicated that their algorithm should be real-time realizable in a smartphone, it is not clear if such algorithm could run in a low-power embedded system. Furthermore, the method for performance evaluation is questionable as well - the sample of 25 subjects before and after cardioversion is not adequate to make a strong conclusion.

### 1.2.3 Quality Assessment of the Photoplethysmogram Signal

The signal quality always comes into question when monitoring in long-term. The PPG is widely-known for its quality being easily degraded by motion artifacts. Therefore, the quality assessment of the PPG is especially important. The existing methods are either feature-based or template-based. The feature-based algorithms extract some features of the PPG (such as rising / falling slope count, heart rate, etc.) and compare them to threshold values, which indicate normal PPG signal [34, 35]. Although such algorithms require low computational resources and work well for normal PPG signals, they are not suitable for distinguishing between PPG during arrhythmia and motion artifacts. As we have already seen, the PPG morphology during AF is very different to that during normal rhythm. Therefore, feature-based algorithms might create a lot of false alarms of low-quality-PPG during AF.

The template-based algorithms compare each PPG pulse to the template of the ideal PPG signal and decide if it is PPG pulse or motion artifact [36]. The comparison usually requires cross-correlation and time-warping due to quasiperiodicity of PPG, therefore, such algorithms are very demanding computationally. On the other hand, if machine learning algorithms are used for setting the thresholds, arrhythmic PPG signals could be used as well. Then, the algorithm would be able to distinguish not only between normal PPG and motion artifact, but also between motion artifact and PPG during AF.

### 1.2.4 Considerations for Implementation in an Embedded System

Since hemodialysis procedure should be stopped when AF occurs, the real-time AF detection is desired. In order to implement the algorithm in real time we need to take into account the requirements of the embedded system. The computational requirements of the algorithm must not exceed certain thresholds regarding the processing time and memory. The data should be processed in a sliding window. Ideally, sample-by-sample operation is desired in order to reduce memory size. Furthermore, sample-by-sample operation can be always applied for a processing of a bigger buffer, while the vice versa transformation is not necessary possible. An example of a real-time implementation could be an integrated circuit [37]. Such integrated solution is interesting due to extremely low energy operating voltage (290 mV). Such voltage reduction showed energy savings of up to 41 times, when compared to nominal 1.2 V operating voltage.

### 1.2.5 Signal Databases

The most popular database with atrial fibrillation is *MIT-BIH Atrial Fibrillation Database* [38]. This database includes 25 ECG recordings of human subjects with AF. The recordings are 10 hours in duration and contain two ECG signals sampled at 250 samples per second, 12-bit resolution with bandwidth from 0.1 to 40 Hz.

Another popular database is *The Long-Term AF Database* [39]. It contains 84 long-term ECG recordings with paroxysmal and sustained AF. Each recording is typically 24 to 25 hours in duration and contains two ECG signals sampled at 128 samples per second, 12-bit resolution.

Unfortunately, annotated PPG signal databases with AF episodes are not publicly available. *The MIMIC Database* [40] and *MIMIC II Waveform Database* [41] contain records from the patient monitors in intensive care units. *The MIMIC Database* contain over 90 recordings. Each recording contain various signals from the patient monitor and is at least 20 hours long resulting in total of nearly 200 patient-days of signals. *The MIMIC II Waveform Database* contains 23180 sets of recordings and over 3 TB data in total. The recordings contain several signals from the patient monitor, including ECG, PPG, blood pressure and respiration. Although the mentioned MIMIC databases include PPG signals, they are not annotated regarding arrhythmias.

# 2. Methods and Materials

This chapter presents methodology of the work including the algorithm for signal processing, the description of the collected signals, considerations regarding the implementation in the embedded system, and the methods for performance evaluation.

## 2.1. The Proposed Algorithm for Atrial Fibrillation Detection

This section presents the algorithm for atrial fibrillation detection using solely the PPG signal. First, a short overview is presented, followed by more detailed explanation of each building block.

### 2.1.1 Structure of the Proposed Algorithm

Figure 2.1 shows the block diagram of the proposed algorithm. In the preprocessing stage, a low-pass filter with cut-off frequency $f_c$ is used to suppress high frequency noise [42]. Then, an adaptive filter based on least mean squares (LMS) is used to remove the baseline wander from the PPG signal. Parameters of the filter consist of one adaptive coefficient $\omega_1$ and the adaptation step $\mu$ [21]. The resulting PPG signal without the baseline wander $p_a(n)$ branches into two routes. In one way, the $p_a(n)$ is further passed on to the peak detector, which refers to [43]. The first step in peak detection is slope sum function (SSF) with window length $N$. The output of the SSF $s(n)$ is compared with threshold $T$. The threshold $T$ is updated based on a median $a_m(m)$ of the amplitude $a(m)$ of the last five peaks found. For each peak found the index $i(m)$ is noted and peak-to-peak interval $\Delta i(m)$ is calculated. Finally, the AF detector, presented in [32], takes place for decision making. This detector was originally used for analysis of RR intervals obtained from the ECG. In the current work, we adapted the

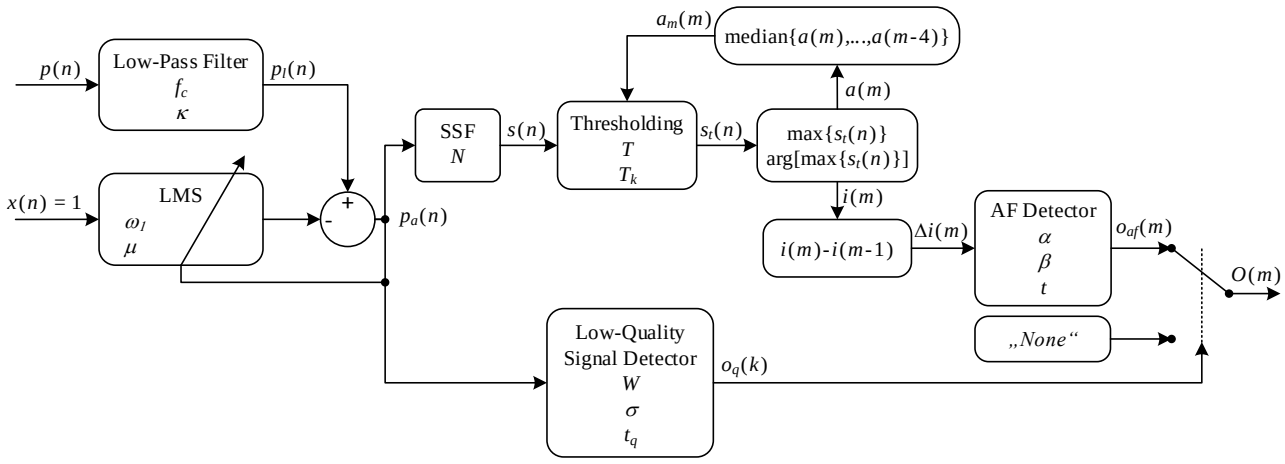


Figure 2.1: Overall structure of the algorithm

algorithm to analyze interval series, extracted from the PPG. The detector is characterized by three parameters: $\alpha$ - the smoothing factor, $\delta$ the bigeminy (every second beat is a premature beat) suppression threshold, and $t$ - the threshold to produce the binary output. The binary output of this detector $o_{af}(m)$ has two states: „AF“ for atrial fibrillation and „Normal“ for normal rhythm. The last block in the diagram is for signal quality evaluation. The preprocessed PPG $p_a(n)$ is passed as the input to this block. The low-quality-signal detector is characterized by three parameters: $W$ - the window length, $\sigma$ - smoothing factor, $t_q$ - threshold to produce binary output. The output of this detector ($o_q(k)$) has two states: „High“ for the high-quality signal „Low“ for the low-quality signal. The signal quality meter controls the output switch of the entire algorithm. It connects the final output $O(m)$ to either the output of the AF detector or to the state „None“, if the quality of the signal is not sufficient. It should be noted that there are three different sampling indexes: $n$ - representing the $n$th sample in the PPG, $m$ - representing the $m$th peak-to-peak interval, and $k$ - representing the $k$th sample of the low-quality-signal detector.

### 2.1.2 Photoplethysmogram Preprocessing

The signal preprocessing stage consists of two parts: a low-pass filter for high frequency noise removal and an adaptive high-pass filter for baseline removal. The low-pass filter [42] is characterized by a cut-off frequency, which is determined by the natural number $\kappa$, representing the power of two (see Fig. 2.2).

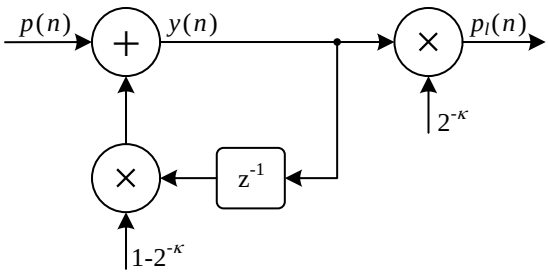


Figure 2.2: Structure of the low-pass filter

The main feature of this filter is the possibility to avoid multiplications and use left or right bit shifts instead. The intermediate output $y(n)$ is calculated by

$$y(n) = (1 - 2^{-k}) \cdot y(n-1) + p(n), \tag{2.1}$$

where $p(n)$ is the raw PPG signal representing the input and $\kappa$ is the integer number which

determines the cut-off frequency. The equation 2.1 is transformed into

$$y(n) = y(n-1) - 2^{-\kappa} \cdot y(n-1) + p(n). \tag{2.2}$$

In this case, we can see that the only required multiplication is between the delayed intermediate output sample and the power of two. This multiplication can be replaced by the right bit shift by $\kappa$ positions. Of course, such replacement could be used only if we are dealing with unsigned integers. However, most of the compilers for embedded systems are capable of optimizing such multiplications with signed integers as well. This operation is optimized by removing the sign bit, applying the shift and placing the shift bit back. The final output of the filter $p_l(n)$ is calculated by

$$p_l(n) = y(n) \cdot 2^{-\kappa}, \tag{2.3}$$

which could be optimized in the same way. The $\kappa$ parameter of the filter used in this work is equal to 2, which represents the cut-off frequency of $0.047 \cdot F_s$, where $F_s$ is the sampling frequency. With the sampling frequency of 125 Hz, the $f_c = 5.8$ Hz. The rough estimate of the cut-off frequency from the amplitude frequency response is 5.7 Hz (see Fig. 2.3). The estimates of cut-off frequency depending on the parameter $\kappa$ for such filter are presented in Table 2.1. The phase response is close to linear in the pass-band (see Fig. 2.3). Non-linear phase out of the pass-band is acceptable, since the most of the spectral energy of PPG is condensed in the pass-band. Figure 2.4 shows an example of the behavior of the described low-pass filter. The contaminated input signal $p_n$ is a sum of high-quality PPG signal $p$ and white Gaussian noise. We can see that the filter performs adequately without visibly distorting the initial PPG signal.

Table 2.1: Normalized bandwidth of the low-pass filter depending on the value of $\kappa$

| $\kappa$ | Bandwidth (normalized to 1 Hz) | Bandwidth, Hz ($F_s = 125$ Hz) |
|---|---|---|
| 1 | 0.120 | 15.0 |
| 2 | 0.047 | 5.8 |
| 3 | 0.022 | 2.7 |
| 4 | 0.010 | 1.3 |

The filter is characterized by the adaptive cut-off frequency, using the LMS algorithm [21]. Therefore, it tracks baseline wander more effectively than the conventional digital filter with a fixed cut-off frequency. The primary input is the PPG signal $p_l(n)$ contaminated by baseline wander. The reference input is a constant value of 1. The output of the filter is the

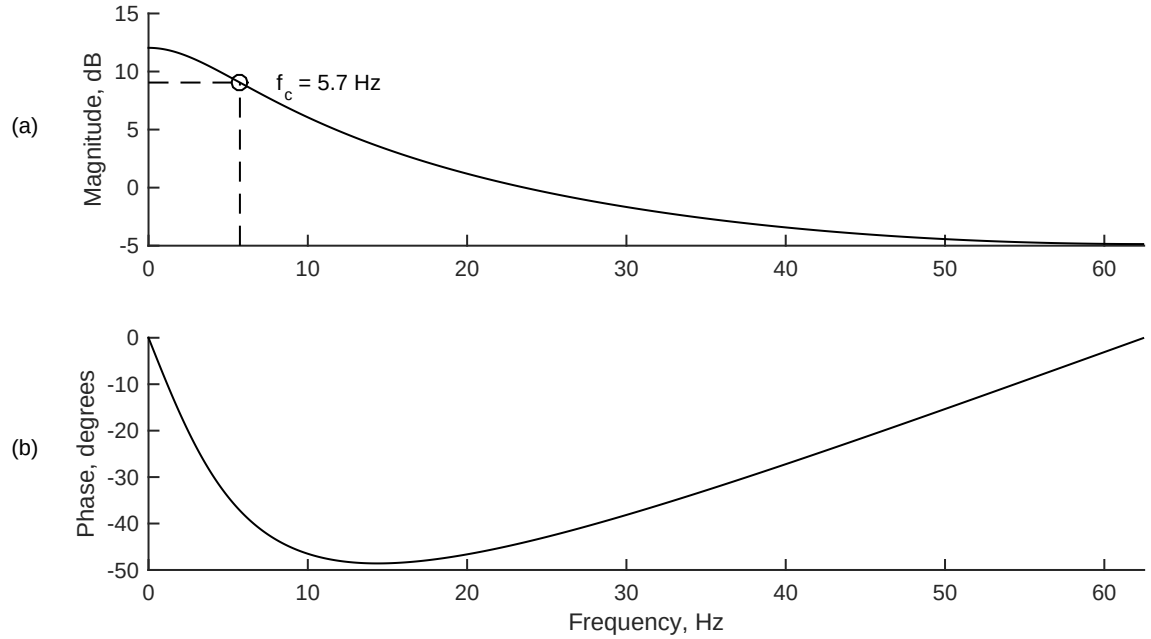


Figure 2.3: Frequency responses of the low-pass filter: (a) amplitude frequency response (the amplification occurs due to missing scaling step); (b) phase frequency response

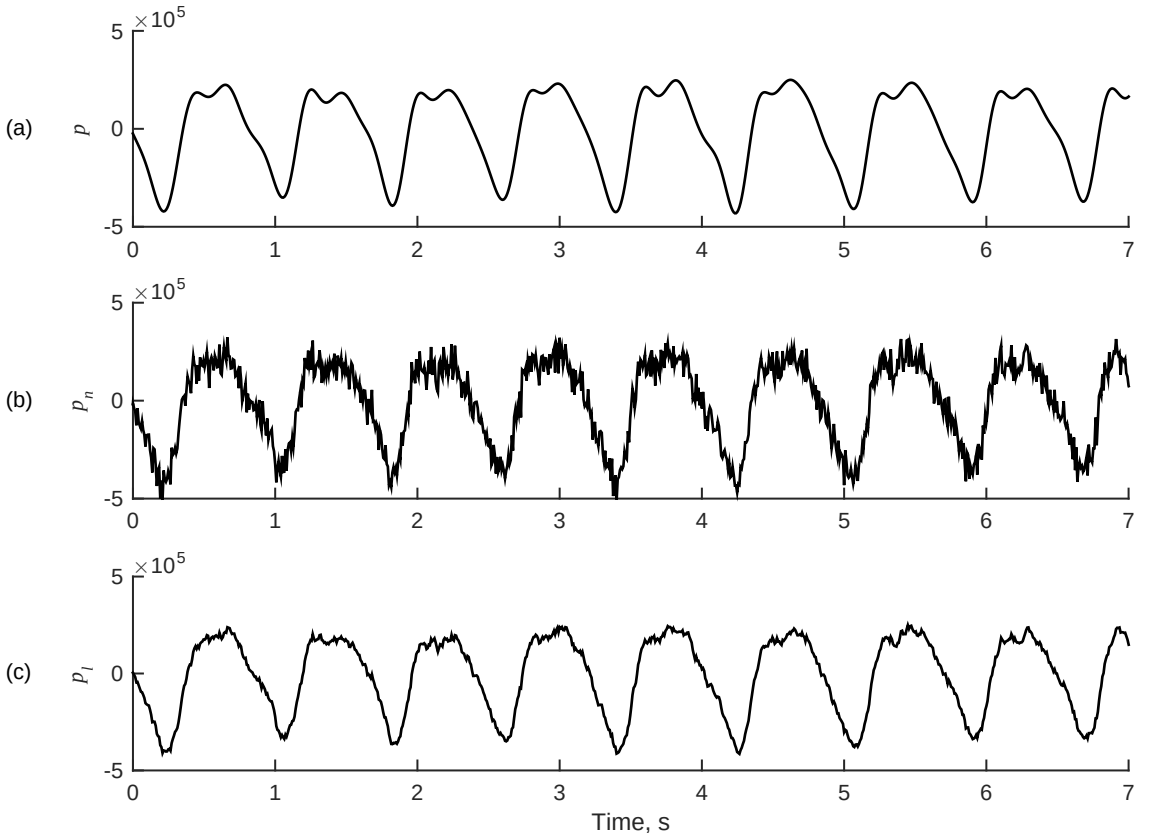


Figure 2.4: (a) PPG without noise; (b) PPG contaminated with high frequency noise; (c) low-pass-filtered PPG

error signal $p_a(n)$, which is calculated by

$$p_a(n) = p_l(n) - w_1(j) \cdot x(n), \tag{2.4}$$

where $w_1(j)$ represents the current weight of the filter. The weight is updated by

$$w_1(j+1) = w_1(j) + 2 \cdot \mu \cdot p_a(n), \tag{2.5}$$

where $w_1(j+1)$ represents the future weight of the filter and $\mu$ is the adaptation step. According to [21], the maximum cut-off frequency $f_m$ of such filter is defined by

$$f_m = \frac{\mu}{\pi} \cdot F_s. \tag{2.6}$$

Selecting $\mu = 0.0195$ and $F_s = 125$ Hz, we get a cuf-off frequency of 0.8 Hz. This means that baseline variations of frequencies higher than 0.8 Hz will remain in the signal. This exact $\mu$ value was determined experimentaly, because it scales-well to an integer value of 20 by a factor of $2^{10}$. It was noted in [21] that this filter significantly distorts the morphology of the signal. Therefore, it could not be applied for ECG processing without limiting the $f_m$ to 0.3 Hz. The distorting effect can be confirmed by an example (see in Fig. 2.5). However, in this particular application, the morphology is not crucial, hence, the filter is suitable for preprocessing the PPG signal.

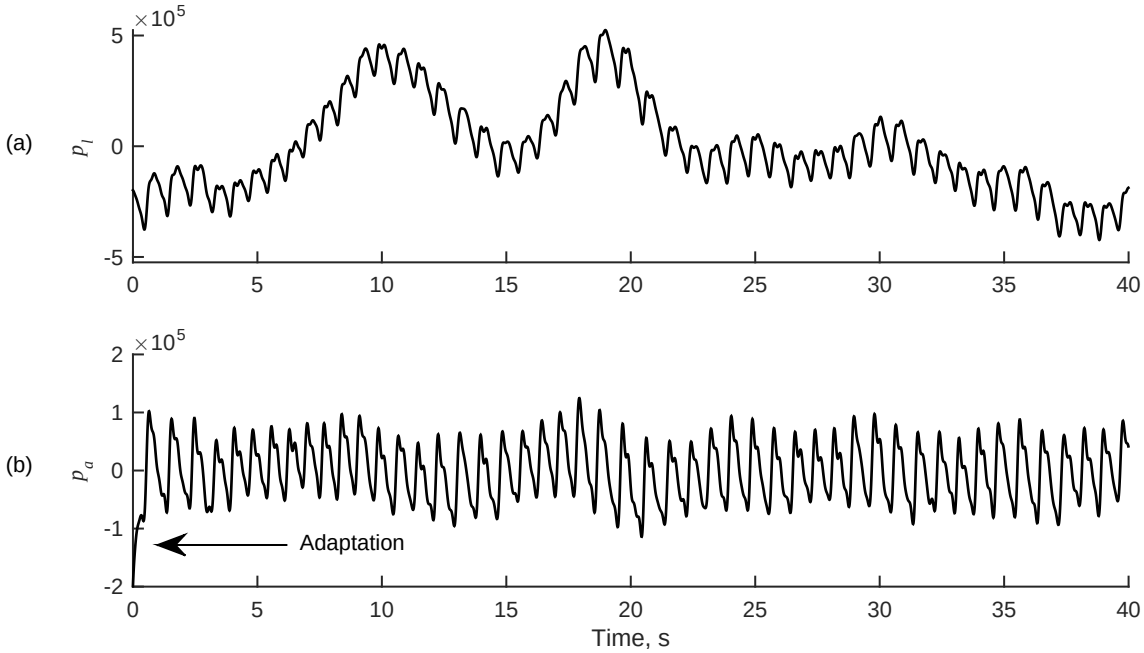


Figure 2.5: (a) PPG with baseline variation; (b) PPG with baseline attenuated by adaptive filter

### 2.1.3 Peak Detection in Photoplethysmogram

The key feature of the peak detection block is the slope sum function [43] with a window size of $N$ samples. The input signal $p_a(n)$ is transformed into a series of pulses. The output

of the slope sum function $s(n)$ is defined by

$$s(n) = \sum_{k=n-N+2}^{n} \Delta p_a(k) \cdot H(\Delta p_a(k)), \tag{2.7}$$

where $H(\cdot)$ is the Heaviside step function and the difference $\Delta p_a(k)$ is calculated by

$$\Delta p_a(k) = p_a(k) - p_a(k-1). \tag{2.8}$$

Therefore, the output of the slope sum function is the sum of increasing slopes in the specified window. Each of the pulses of the output has a clearly expressed maximum with a single extremum. Such pulses are well-suited for threshold-based peak detection. The threshold is calculated by

$$T(m) = a_m(m) \cdot T_k, \tag{2.9}$$

where $T_k$ is a threshold coefficient between 0 and 1 and $a_m(m)$ is the amplitude of the representative peak found. The latter is the output of 5-samples median filter

$$a_m(m) = median\{a(m), a(m-1), a(m-2), a(m-3), a(m-4)\}, \tag{2.10}$$

where $a(m)$ is the amplitude of the current peak detected. The decision algorithm identifies if the current sample is the peak based on several rules. At the beginning, there is an initialization process required to identify the initial amplitude $a(m)$ for the threshold. It is selected as the maximum in a window which starts from the 50th sample and ends at the 187th sample. The starting point of the window represents empirically determined period of adaptation of the adaptive filter. In some cases, when the adaptation has a rising slope (as in Fig. 2.5), the output of the slope sum function has an inadequately high peak. Therefore, this period could not be considered for the initial threshold amplitude. The ending point of this window was chosen so that at least one PPG pulse would be included in the window. It was determined by the lowest possible normal heart rate of 40 bpm. To detect a peak, a window of 3 samples is continuously being processed. If the middle sample is higher than the first sample, and lower than the last sample, the middle sample is identified as a peak. Additionally, the new peak-to-peak interval is calculated instantly. It is used to prevent peaks that would result in intervals shorter than the lowest possible interval corresponding to the heart rate of 300 bpm. Furthermore, only one peak is allowed between two zero points in the output of the SSF. Normally, there is a zero-level period in the $s(n)$ signal, since the falling slope is similar to the rising slope. However, when sufficient amount of noise

is present, the morphology of the pulses in the $s(n)$ include several peaks. When a new peak is confirmed, a new peak-to-peak interval $\Delta i(m)$ is calculated.

Figure 2.6 presents an example of peak detection with all of the peaks detected correctly. At the beginning, a false peak in $s(n)$ can be seen. As mentioned, this occurs during the adaptation of the adaptive filter. The initialization period is denoted. We can see how the threshold is being updated. The peak-to-peak intervals are calculated starting from the second peak found. The overall initialization period for peak detection lasts up to 3 seconds in this particular case.

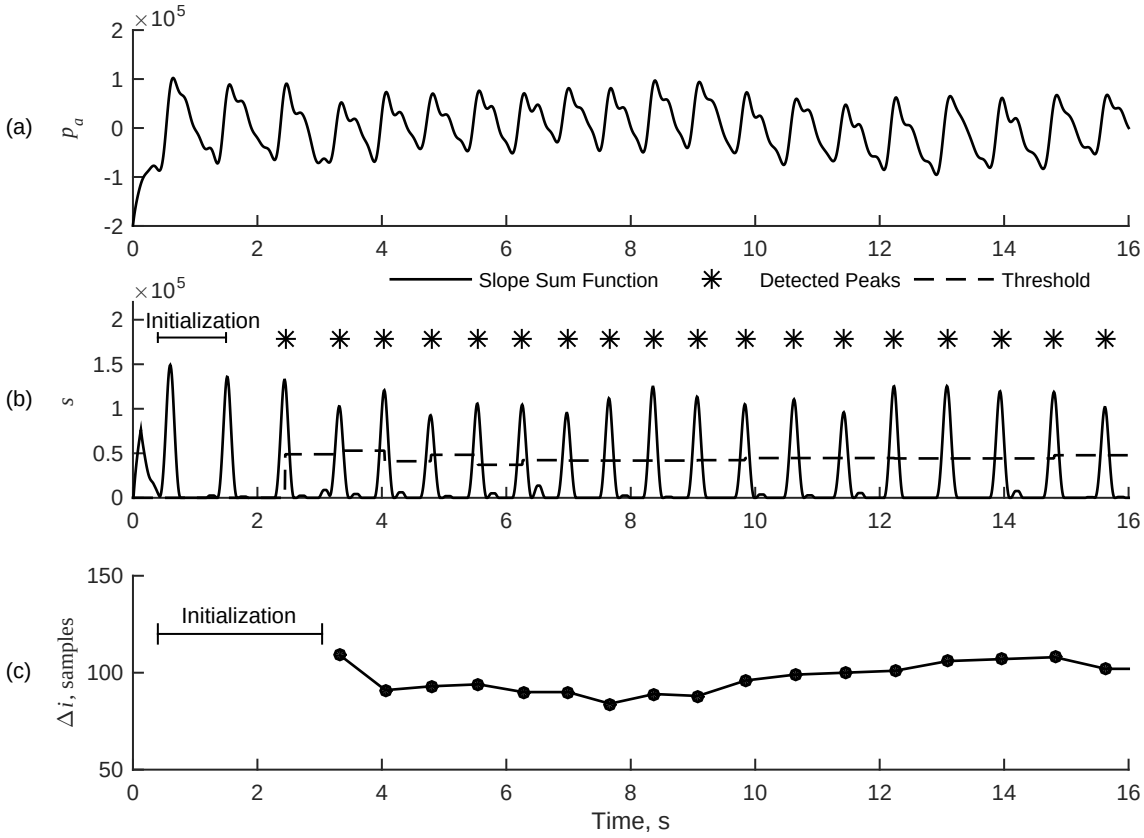


Figure 2.6: (a) PPG with baseline removed; (b) output of the slope sum function, adaptive threshold, and the detected peaks; (c) resulting peak-to-peak intervals

### 2.1.4 Pulse-Based Atrial Fibrillation Detection

One of the key building blocks of the proposed algorithm is the low-complexity AF detector (see Fig. 2.7), presented in [32]. The detector was originally developed for the analysis of RR intervals obtained from the ECG. In the current work, we adapted this algorithm to analyze hearth rhythm series, extracted from the PPG.

A 3-point median filter is used to reduce the influence of ectopic beats. The filter is defined by

$$r_m(m) = median\{\Delta i(m), \Delta i(m-1), \Delta i(m-2)\}, \tag{2.11}$$

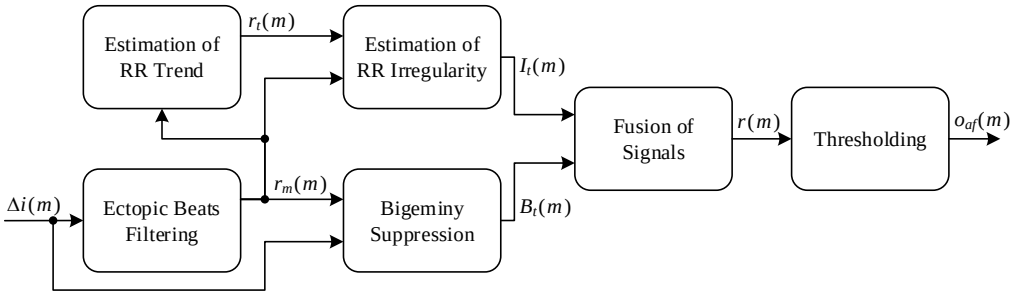


Figure 2.7: Structure of the AF detector

where $i(m)$ denotes the length of the $m$th peak-to-peak interval. Such filter is also useful for removing incorrect intervals due to falsely detected or undetected peaks. The exponential averager is used to track the trend in the peak-to-peak interval series. The exponential averager is defined by

$$r_t(m) = \alpha^2 \cdot \Delta i(m) + 2 \cdot (1-\alpha) \cdot r_t(m-1) - (1-\alpha)^2 \cdot r_t(m-2), \tag{2.12}$$

where $\alpha$ is the smoothing factor. To detect the irregularity of the peak-to-peak intervals detector employs a simple measure similar to sample entropy estimation. All pairwise peak-to-peak interval combinations are considered. The count $M(i)$ in a window of length $L$ is increased by one, if the difference of the pairwise combination is greater than the difference threshold $\gamma$. The count is normalized with its maximum value $L(L-1)/2$. The count is defined by

$$M(m) = \frac{2}{L(L-1)} \sum_{j=0}^{L-2} \sum_{u=j+1}^{L-1} H(|\Delta i(m-j) - \Delta i(m-u)| - \gamma). \tag{2.13}$$

where $H(\cdot)$ is the Heaviside function. The property of interval irregularity $I_t(m)$ is defined as a ratio between averaged version of $M(m)$ and interval trend $r_t(m)$ by

$$I_t(m) = \frac{M_t(m)}{r_t(m)}, \tag{2.14}$$

where $M_t(m)$ is a smoothed version of $M(m)$. Another problem regarding the AF detection is bigeminy, which are usually incorrectly interpreted as AF. Another measure of interval irregularity was introduced in [32] and defined by

$$B(m) = \left( \frac{\sum_{j=0}^{E-1} r_m(m-j)}{\sum_{j=0}^{E-1} \Delta i(m-j)} - 1 \right)^2, \tag{2.15}$$

where $E$ is an even-valued integer. Similar to $r_t(m)$ and $M_t(m)$, $B_t(m)$ is obtained by the exponential averaging of $B(m)$. The ratio in Equation 2.15 is close to one for regular rhythms

and for bigeminy, because $r_m(m)$ and $r(m)$ are similar. However, for AF the ratio becomes lower than one, because $r_m(m)$ is smaller than $r(m)$. The final step is a simple signal fusion procedure defined by

$$r(m) = \begin{cases} I_t(m), & \text{if} \quad B_t(m) \geq \beta \\ B_t(m), & \text{otherwise,} \end{cases} \tag{2.16}$$

where $r(m)$ is the continuous output of the algorithm, and $\delta$ is the threshold for bigeminy suppression. If the threshold $t$ is applied, as defined by

$$o_{af}(m) = \begin{cases} AF, & \text{if} \quad r(m) \geq t \\ Normal, & \text{otherwise,} \end{cases} \tag{2.17}$$

the output becomes binary with the states „AF“ and „Normal“. An example of the behavior of the algorithm is presented in Figure 2.8. The initialization period of $L$ intervals can be clearly seen.

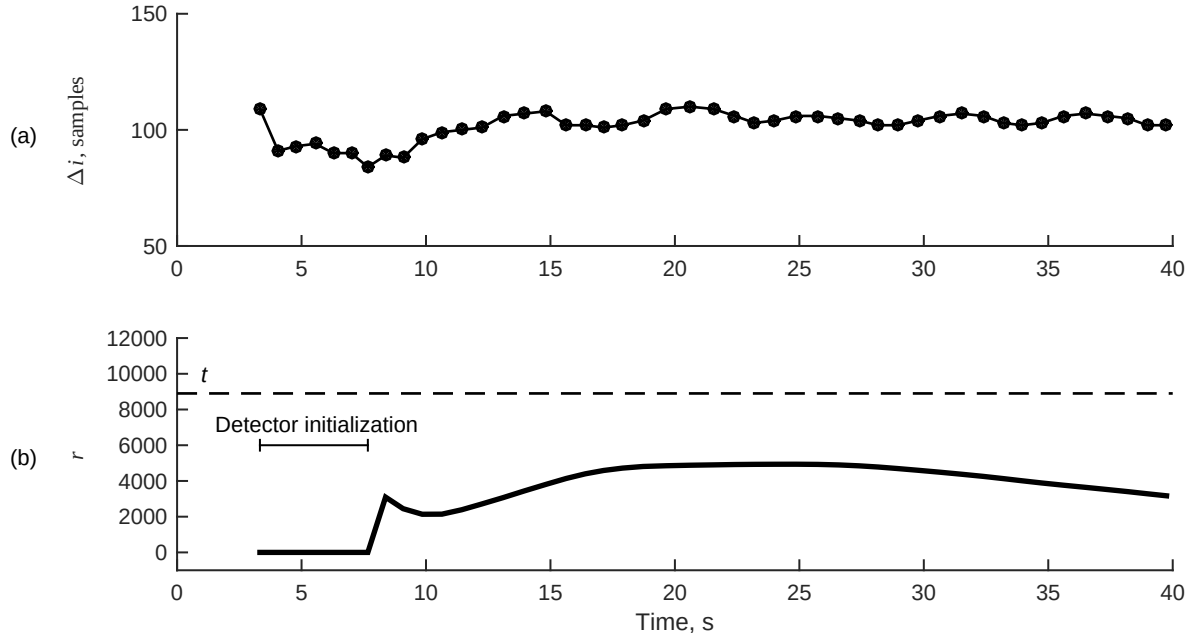


Figure 2.8: Pulse-based AF detection during normal rhythm: (a) peak-to-peak intervals as the input to the AF detector; (b) continuous output of the AF detector and the threshold

### 2.1.5 Low-Quality-Photoplethysmogram Detection

This subsection introduces a method for low-quality-signal detection, which does not require high computational resources. The main idea of this algorithm is to determine the quasiperiodicity of the signal using zero-crossing rate, which is widely-known in speech processing for distinction between speech and non-speech intervals [44]. Instead of zero-

crossing rate we propose a mean-crossing rate. The main advantage is that the signal is not required to be zero-centered as it is for the zero-crossing rate. The input to the low-quality-signal detector is the PPG with removed baseline $p_a(n)$ (see Fig. 2.9).

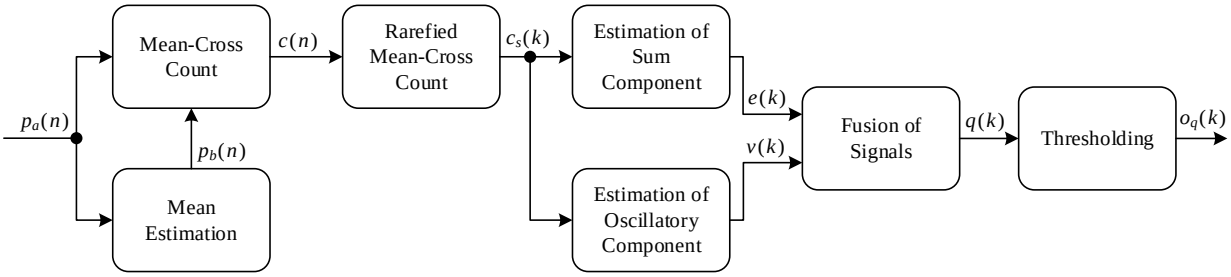


Figure 2.9: Structure of the algorithm for signal quality assessment

At first, the mean of the signal must be determined. It is accomplished using moving mean filter, which is described by

$$p_b(n) = \frac{1}{W} \sum_{j=n-W+1}^{n} p_a(j), \tag{2.18}$$

where $W$ is length of the window. Then, a number of instances, where the PPG signal $p_a(n)$ crosses its mean $p_b(n)$ is defined by

$$c(n) = \sum_{j=n-W+2}^{n} b(j), \tag{2.19}$$

where $b(j)$ is defined by

$$b(j) = \begin{cases} 1, & \text{if} \quad \{p_a(j) \geq p_b(n)\} \wedge \{p_a(j-1) \leq p_b(n)\} \\ 1, & \text{if} \quad \{p_a(j) \leq p_b(n)\} \wedge \{p_a(j-1) \geq p_b(n)\} \\ 0, & \text{otherwise.} \end{cases} \tag{2.20}$$

After that, $c(n)$ has the length of the window $W$. However, there are episodes where $c(n)$ remains constant, while we are interested only in dynamics of this signal. Therefore, a rarefaction is applied to keep only the samples which indicate a change in the signal. The rarefied version $c_s(k)$ is defined by

$$c_s(k) = \begin{cases} c(n), & \text{if} \quad c(n) \neq c(n-1) \\ \varnothing, & \text{otherwise,} \end{cases} \tag{2.21}$$

where $k$ denotes a new sample number and is incremented according to

$$k = \begin{cases} k+1, & \text{if} \quad c(n) \neq c(n-1) \\ k, & \text{otherwise.} \end{cases} \tag{2.22}$$

After this simplification, the time domain of the signal loses linearity. Each new output of the low-quality-signal detector comes with an increment of $k$. Two features are proposed to quantify the mean-cross signal $c_s(k)$: an estimate of the total sum $e(k)$, and an estimate of oscillatory component $v(k)$. The preliminary results showed that the mean-cross rate remain constant with a variation of one or two instances during both -normal rhythm and AF. Due to low quasiperiodicity of PPG signal during AF, the variation is slightly higher for AF signals. However, during the motion artifacts, the range of variation of the mean-cross rate increases significantly. The estimate of sum component $e(k)$ is defined as an absolute sum by

$$e(k) = \sum_{j=k-I+1}^{k} |c_s(j)|, \tag{2.23}$$

where $I$ is the length of a window of $c_s(k)$ samples. The estimation of a oscillatory component is defined by

$$v(k) = \sum_{j=k-I+Z}^{k-1} \delta \left( \sum_{u=j-Z}^{j-1} [c_s(u+1) - c_s(u)] \right), \tag{2.24}$$

where $Z$ is an even-valued integer - the length of a smaller inner window for sum calculations, and $\delta$ is the Kronecker delta function. The argument of the $\delta$ function describes the sum of differences in a window of even-valued length. The idea behind this is that such sum for a fast-varying symmetrical signal would result in exactly zero. While for a slow-varying unsymmetrical signal it would result in approximation of the signal. The outer sum and the Kronecker delta function count the instances of zero-valued results in the overall window of size $I$. Signal fusion of the two features is employed to produce the decision function $q(k)$. The signal fusion is defined by

$$q(k) = \frac{e(k)}{v(k)}. \tag{2.25}$$

For a normal PPG signal (see Fig. 2.10), the oscillatory component is higher than the sum component and the $q(k)$ decreases. For a motion artifact, the oscillatory component is smaller than the sum component and the $q(k)$ increases. The binary output of the low-

quality-signal detector is defined by

$$o_q(k) = \begin{cases} High, & \text{if} \quad q(k) \leq t_q \\ Low, & \text{otherwise.} \end{cases} \tag{2.26}$$

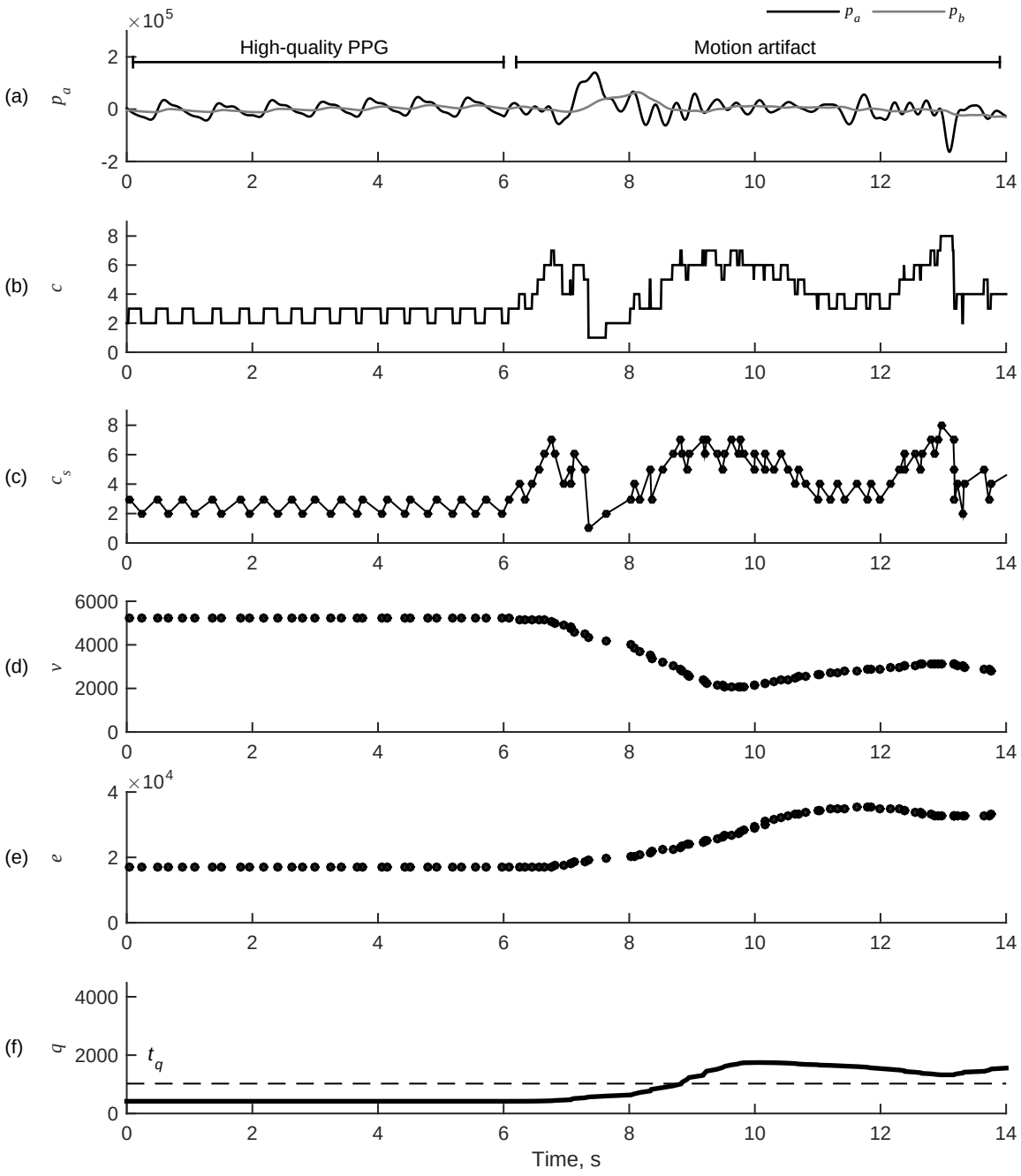


Figure 2.10: PPG signal quality estimation: (a) PPG after adaptive filter and the averaged PPG; (b) baseline cross count; (c) simplified baseline cross count; (d) estimate of the oscillatory component; (e) estimate of the sum component; (f) decision function and threshold for high quality signal

## 2.2. Signals for Performance Evaluation

This section presents the data sources used for the performance evaluation of the proposed algorithm. First, we describe the public database, namely MIMIC, and the records which were used. Then, we describe the noise modeling procedure which is used for evaluation of the proposed method in noisy situations.

### 2.2.1 Clinical Photoplethysmogram Signals

A set of signals was collected from MIMIC signal database [40, 45] for evaluation purposes. This database contains records with synchronously recorded ECG and PPG signals, sampled at 125 samples per second. The signals are not annotated in terms of arrhythmia. We have collected a set of 2200 signals of which each is 1 minute in duration. Half of the signals are with atrial fibrillation and the other half represent normal rhythm. We have identified signals of atrial fibrillation based on the irregularity of the heart rhythm, the absence of P waves and the presence of fibrillatory f waves in the ECG. The information about the records, which were used for the collection of the signal set is presented in Appendix No. 1. The merged cells on age and sex indicate that several records were obtained from the same patient. The average age in the AF group was $76.7 \pm 7.1$ years, while in the normal rhythm group it was $66.2 \pm 15.8$ years. The AF group included 5 male and 5 female patients, while the normal rhythm group included 11 male and 13 female patients. Two of the records, namely 231m, 276m, were included in both - AF and normal rhythm categories.

### 2.2.2 Modeling of Motion Artifacts

The signals in the selected set from MIMIC database are high quality and contain no movement artifacts in the PPG. However, under real life conditions, the PPG signals are usually contaminated with motion artifacts. Hence, the noise modeling (see Fig. 2.11) was used to investigate the performance of the algorithm with low-quality PPG signals. Since motion artifacts are mostly impulse-like, we used an additive Laplace noise model. The initial step in noise modeling is defined by

$$l(n) = z - w \cdot sign(\upsilon(n)) \cdot ln(1 - 2 \cdot |\upsilon(n)|), \tag{2.27}$$

where $l(n)$ is the $n$th sample of the Laplace-distributed noise, $\upsilon(n)$ is the $n$th sample of the noise uniformly distributed between $-0.5$ and $0.5$, $z$ and $w$ are parameters of the Laplace-distributed noise. The Laplace-distributed noise $l(n)$ was forth-and-back-filtered with 6th

order Butterworth low-pass filter with cut-off frequency of 5 Hz and normalized by its standard deviation. The normalized noise $\mathbf{l_n}$ is defined by

$$\mathbf{l_n} = \frac{\mathbf{l} - \bar{l}}{\sigma_l}, \tag{2.28}$$

where $\bar{l}$ is the mean value of $\mathbf{l}$ and $\sigma_l$ is the standard deviation of $\mathbf{l}$. The PPG was scaled to extend over the range of 20-bit signed integer and then normalized to mean to be equal to zero. The PPG scaling to 20-bit range is defined by

$$\mathbf{p_s} = \begin{cases} \mathbf{p_m} \cdot \frac{(2^{19}-1)}{|\max[\mathbf{p_m}]|}, & \text{if} \quad |\max[\mathbf{p_m}]| \geq |\min[\mathbf{p_m}]| \\ \mathbf{p_m} \cdot \frac{(2^{19}-1)}{|\min[\mathbf{p_m}]|}, & \text{otherwise,} \end{cases} \tag{2.29}$$

where $\mathbf{p_m}$ is the raw PPG signal from the MIMIC database. The constant $2^{19}-1$ represents the maximum value for a 20-bit signed integer. Then, the noise was scaled according to desired signal-to-noise ratio (SNR) level. The scaled noise is defined by

$$\mathbf{l_s} = \mathbf{l_n} \cdot 10^{-\frac{S}{20}} \cdot \sigma_p, \tag{2.30}$$

where $S$ is the desired SNR level in dB and $\sigma_p$ is the standard deviation of $\mathbf{p_s}$. Then the intermediate contaminated PPG signal $\mathbf{p_x}$ is defined by an additive model

$$\mathbf{p_x} = \mathbf{l_s} + \mathbf{p_s}. \tag{2.31}$$

Additionally, the saturation was implemented to prevent values higher than the ones possible in hardware (out of 22-bit range). The saturation operation is defined by

$$p_x(n) = \begin{cases} 2^{21}-1, & \text{if} \quad p_x(n) > 2^{21}-1 \\ -2^{21}, & \text{if} \quad p_x(n) < -2^{21} \\ p_x(n), & \text{otherwise.} \end{cases} \tag{2.32}$$

where $2^{21}-1$ and $-2^{21}$ represent the extremum values for 22-bit signed integers. Additionally, the baseline variation modeling was implemented. The initial baseline $\mathbf{b_i}$ was modeled as three points from a uniform distribution with mean equal to 0. The $\mathbf{b_i}$ was re-sampled to match the sampling frequency of the PPG signal into $b_r(n)$. The re-sampled baseline $\mathbf{b_r}$ was

scaled according to the 22-bit range and the range of $p_x(n)$. The scaling is defined by

$$\mathbf{b_s} = \mathbf{b_r} \cdot \frac{2^{21} - 1 - \max[\mathbf{p_x}] + 2^{21} + \min[\mathbf{p_x}]}{\max[\mathbf{b_r}] - \min[\mathbf{b_r}]}. \tag{2.33}$$

The final contaminated PPG signal $p_n(n)$ is defined by an additive model

$$\mathbf{p_n} = \mathbf{p_x} + \mathbf{b_s}. \tag{2.34}$$

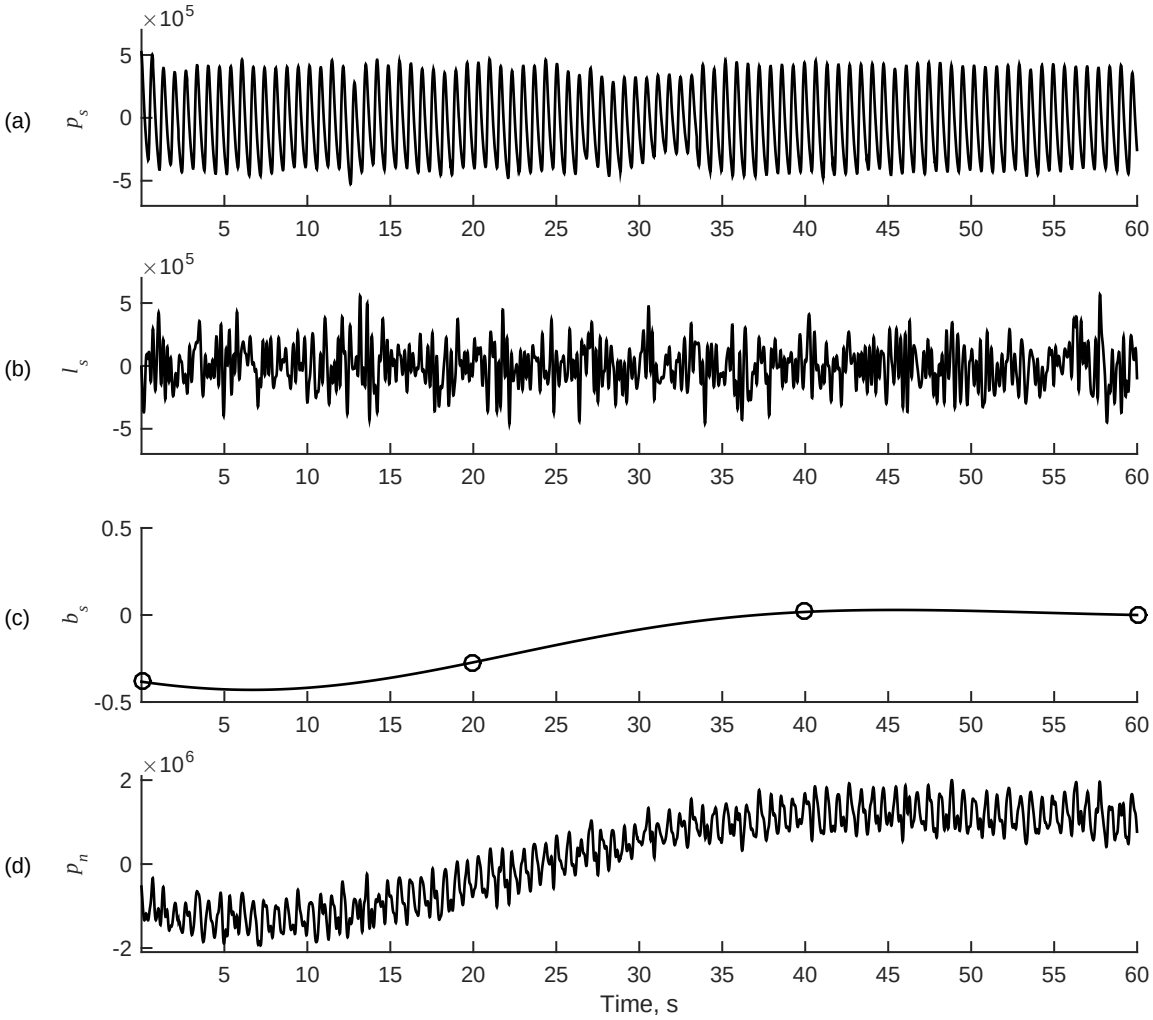


Figure 2.11: Noise modeling approach at SNR level of 5 dB: (a) scaled PPG signal, (b) low-pass-filtered noise from Laplace distribution, (c) modeled baseline with its initial points, (d) the final PPG with noise and baseline wandering

### 2.2.3 Photoplethysmogram Acquisition from Healthy Subjects

Signals were also recorded using a wearable device developed in Biomedical Engineering Institute at Kaunas University of Technology. The wearable device is capable of recording PPG at 100 samples per second. Five healthy subjects participated in the signal acquisition.

A PPG signal under low activity condition was recorded for each subject. The recording lasted for one hour for each subject. Additionally, one 10-minute-long PPG signal was recorded, containing both - high- and low-quality PPG signal.

One additional signal was recorded from a patient with AF in *Hospital of Lithuanian University of Health Sciences Kauno Klinikos*. The recording was accomplished using another device developed in Biomedical Engineering institute at Kaunas University of Technology [46].

## 2.3. Embedded System and Real-Time Implementation

We propose that AF monitoring and detection could be accomplished by using a wearable PPG device developed in Biomedical Engineering Institute at Kaunas University of Technology [47]. The wearable PPG device (see Figure 2.12) is capable of recording physiological data as well as processing it. It is capable of recording:

- PPG,
- galvanic skin response,
- skin temeprature,
- skin humidity,
- accelerations in 3 axes,
- angular velocity in 3 axes,
- atmospheric pressure.

The key features of the device regarding the acquisition of PPG and real-time signal processing include:

- ARM Cortex-M0 Core, running at 16 MHz;
- SRAM with size of 16 kB;
- program memory with size of 128 kB;
- 2.4 GHz transceiver supporting Bluetooth v4.0;
- AFE4490 front-end for PPG acquisition;
- Li-ion battery with capacity of 610 mAh;

The values for parameters of the algorithm are summed up in Table 2.2. Most of the tunable parameters were determined empirically, except for the parameters of AF detector, which were taken from [32].

Additional scaling was required in order to implement the algorithm with integer values. Where possible, scaling coefficients were selected as the power of two due to faster multiplication and division. First of all, the adaptation step was scaled by $2^{10}$, with $\mu = 0.0195$, the scaled value of $\mu$ became equal to 20. The value of $2^{10}$ correspond to the difference in

Figure 2.12: The wearable PPG wearable device: front (left) and back (right)

Table 2.2: Values for real-time implementation of the algorithm

| Parameter | Value | Units | Note |
|---|---|---|---|
| $f_c$ | 5 | Hz | Low-pass filter cut-off frequency |
| $\kappa$ | 2 | - | Related to $f_c$ |
| $\omega_1$ | 0 | - | Initial value |
| $\mu$ | 0.0195 | - | - |
| $N$ | 16 | samples | Window length for SSF |
| $T_k$ | 30 | % | Threshold coefficient |
| $L$ | 8 | samples | Window length for AF detector |
| $\alpha$ | 0.05 | - | Smoothing factor for AF detector |
| $\beta$ | 0.0002 | - | Bigeminy threshold for AF detector |
| $\gamma$ | 0.032 | - | Difference threshold for AF detector |
| $t$ | 0.836 | - | AF detection threshold |
| $W$ | 128 | samples | Window length for signal quality detection |
| $\sigma$ | 0.05 | Hz | Smoothing factor for signal quality detection |
| $t_q$ | 9 | - | Low signal-quality detection threshold |
| $F_s$ | 125 | Hz | Sampling frequency |
| $f_m$ | 0.8 | Hz | Maximum cut-off frequency of adaptive filter |
| $I$ | 17 | samples | Intermediate window length for signal quality detector |
| $Z$ | 4 | samples | Inner window length for signal quality detector |

bit-width between 22-bit PPG values and 32-bit integer values. Therefore, the Equation 2.4 was redefined by

$$w_1(j+1) = w_1(j) + 2 \cdot \mu \cdot 2^{10} \cdot p_a(n), \tag{2.35}$$

and correspondingly the Equation 2.5 was redefined by

$$p_a(n) = \frac{p_l(n) \cdot 2^{10} - w_1(j)}{2^{10}}. \tag{2.36}$$

Regarding the exponential averager defined by Equation 2.12, the $\alpha$ coefficient was not scaled by itself, but rather the final coefficients of the filter were scaled by $2^9$. This value was chosen, since it is the minimum scaling factor required to bring coefficients to integer range, when $\alpha = 0.05$. The calculation of $M(m)$ in Equation 2.13 was redefined by

$$M(m) = \sum_{j=0}^{L-2} \sum_{u=j+1}^{L-1} H(|\Delta i(m-j) - \Delta i(m-u)| - \gamma \cdot 125), \tag{2.37}$$

where the constant 125 corresponds to the sampling frequency in samples per second. The normalization term $2/[L(L-1)]$ was removed as well, since with a fixed window length $L$ the normalization remains constant. The calculation of $B(m)$ was scaled by $2^8$, therefore, the Equation 2.15 was redefined by

$$B(m) = \left( \frac{2^8 \cdot \sum_{j=0}^{E-1} r_m(m-j)}{\sum_{j=0}^{E-1} \Delta i(m-j)} - 1 \cdot 2^8 \right)^2. \tag{2.38}$$

Then, corresponding threshold $\beta$ and values of $I_t(m)$ had to be scaled as well. Therefore, the Equation 2.16 was redefined by

$$r(m) = \begin{cases} I_t(m), & \text{if} \quad B_t(m) \geq \beta \cdot 2^{16} \\ B_t(m), & \text{otherwise,} \end{cases} \tag{2.39}$$

and Equation 2.14 was redefined by

$$I_t(m) = \frac{M_t(m) \cdot 2^{16}}{r_t(m)}. \tag{2.40}$$

The final threshold $t$ had to be scaled as well. Equation 2.17 was redefined by

$$o_{af}(m) = \begin{cases} AF, & \text{if} \quad r(m) \geq t \cdot \frac{2^{16} \cdot 28}{125} \\ Normal, & \text{otherwise,} \end{cases} \tag{2.41}$$

where the constant 28 corresponds to the inverse value of normalization term $2/[L(L-1)]$ from Equation 2.13 and the constant value of 125 corresponds to sampling frequency in samples per second. The final scaling of $2^7$ was required in Equation 2.25 which was redefined

by

$$q(k) = \frac{e(k) \cdot 2^7}{v(k)}. \tag{2.42}$$

The threshold $t_q$ was scaled accordingly, therefore, the Equation 2.26 was redefined by

$$o_q(k) = \begin{cases} High, & \text{if} \quad q(k) \leq t_q \cdot 2^7 \\ Low, & \text{otherwise,} \end{cases} \tag{2.43}$$

## 2.4. Performance Evaluation

The performance of the proposed AF detection part of the algorithm and the low-quality-signal detection part were evaluated separately. The performance of the AF detection part was evaluated in terms of sensitivity ($Se$), specificity ($Sp$), receiver operating characteristic (ROC) and the area under it. These measures were evaluated considering the entire 1-minute-length signal as a single test sample. If the output of the algorithm matched the annotation by more than 50% of the intervals, the entire signal was considered to be identified correctly. Sensitivity was defined by

$$Se = \frac{TP}{TP + FN}, \tag{2.44}$$

where $TP$ is the number of correctly detected AF signals and $FN$ is the number of AF signals detected as normal rhythm signals. Specificity was defined by

$$Sp = \frac{TN}{TN + FP}, \tag{2.45}$$

where $TN$ is the number of correctly detected normal rhythm signals and $FP$ is the number of normal rhythm signals detected as AF signals. The signals from the collected set were contaminated with the modeled artifacts to evaluate the performance of the algorithm at SNR levels between 0 dB (low quality) and 20 dB (high quality). When testing the signals from healthy subjects, the number and duration of false alarms were the main measures.

The performance of the low-quality-signal detector was evaluated in terms of the histogram of the output values of the detector, sensitivity, specificity and ROC. Signals from the collected set were separated in two classes: high quality (SNR = 20 dB) and low quality (SNR = 0 dB). Additionally, a low-quality signal was recorded on a healthy subject to determine the performance with real motion artifacts.

The performance of the system with an embedded version of the algorithm was tested via hardware-in-the-loop methodology. The real embedded system, described earlier, was used.

The patient with AF was simulated using the pre-recorded PPG signal. The goal of such testing was to determine if the algorithm is capable of running in real time in the presented embedded system and if it performs adequately.

# 3. Results

## 3.1. Examples of Noise Influence on Algorithm's Performance

Examples of the behavior of the algorithm for normal rhythm and AF signals are presented in Figure 3.1 and Figure 3.2, respectively. No additional noise in the PPG is present in these examples. The 20 seconds period is displayed starting from the 10th second in order to avoid transient processes in the examples. The PPG with removed baseline is presented

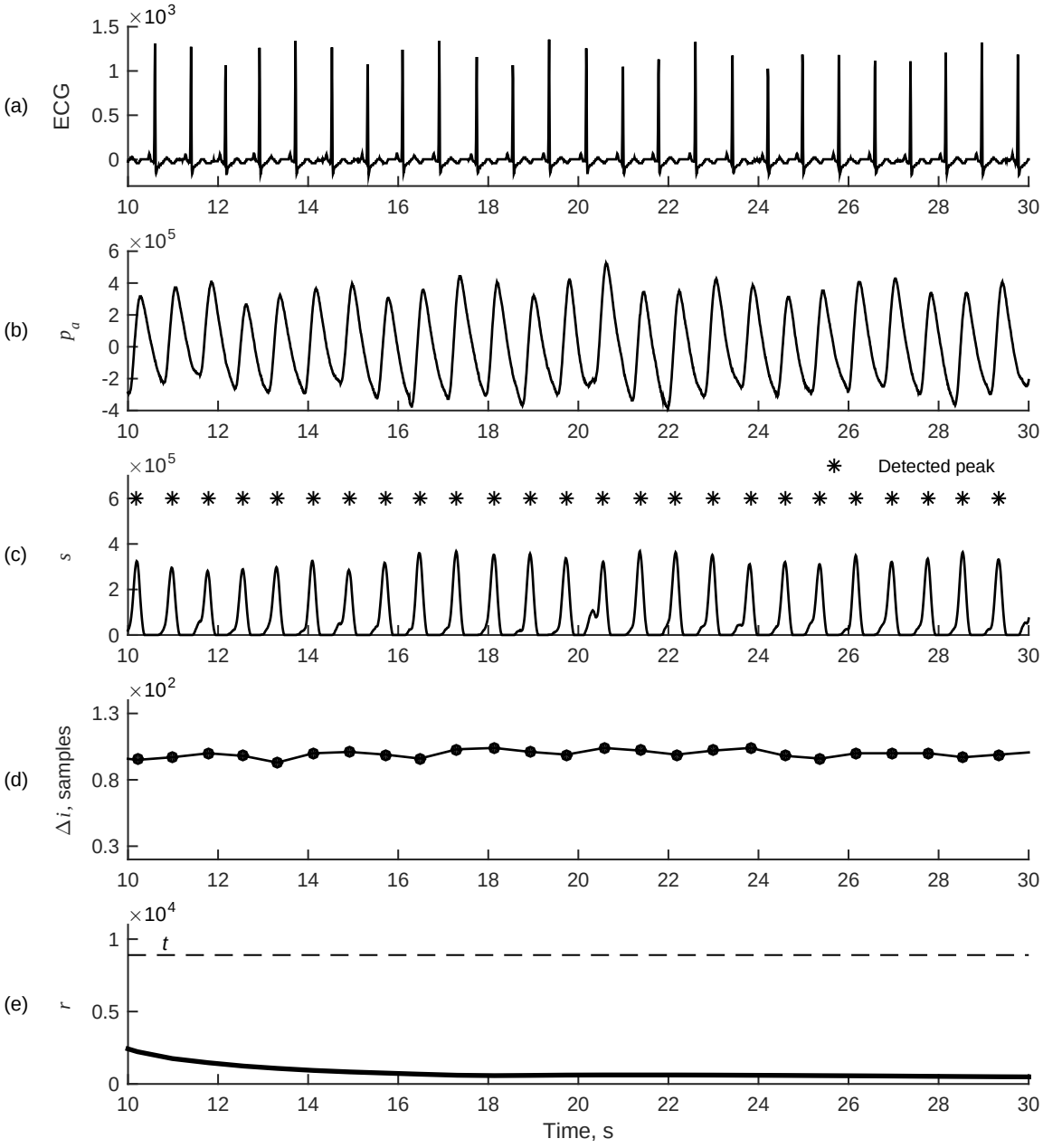


Figure 3.1: Processing of signals with normal rhythm: (a) ECG with removed baseline, (b) PPG scaled to cover the 20-bit integer range, (c) output of SSF and locations of detected peaks, (d) peak-to-peak intervals, (e) continuous output of the algorithm and threshold $t$ for binary output

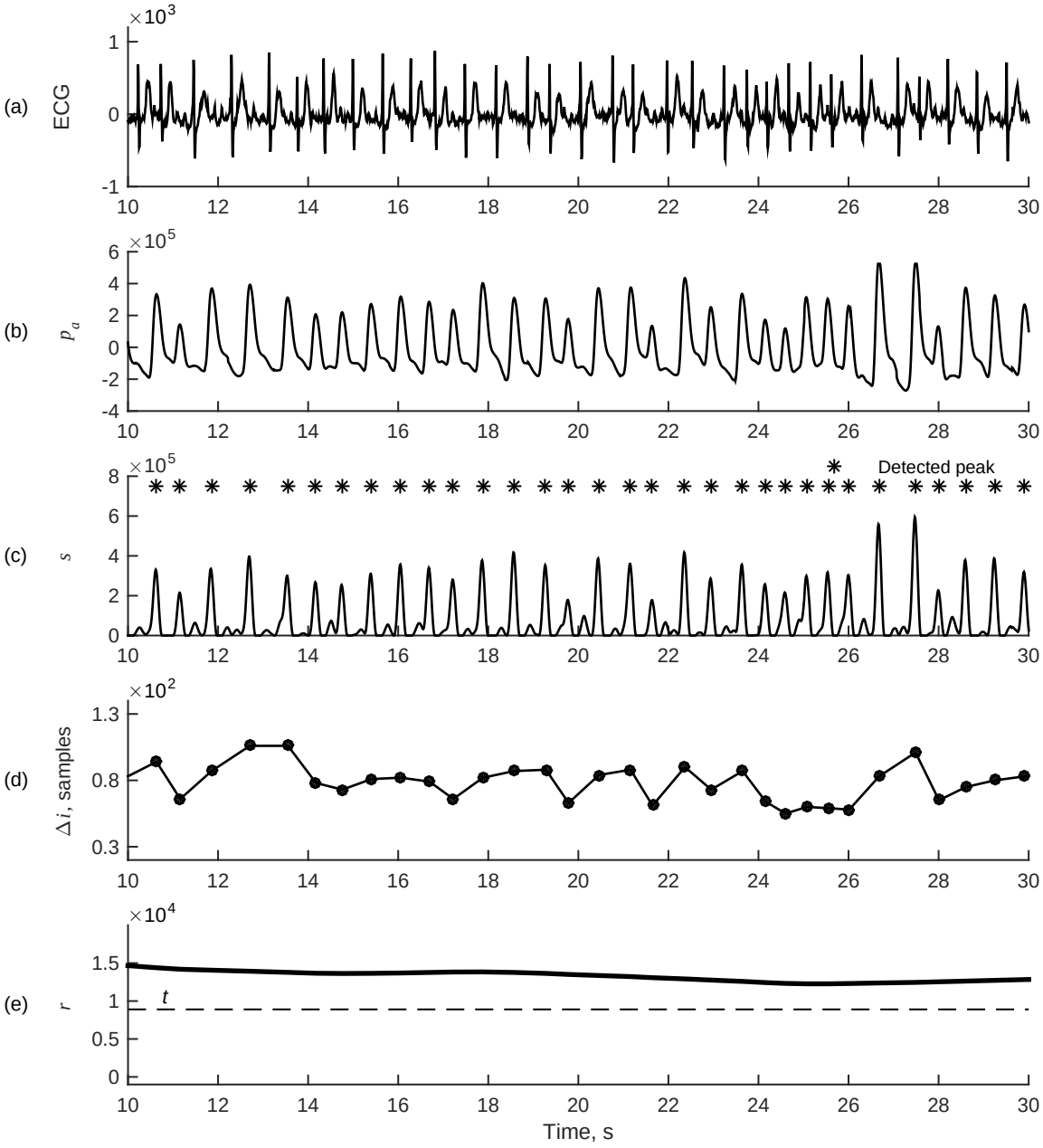


Figure 3.2: Processing of signals with AF: (a) ECG with removed baseline, (b) PPG scaled to cover the 20-bit integer range, (c) output of SSF and locations of detected peaks, (d) peak-to-peak intervals, (e) continuous output of the algorithm and threshold $t$ for binary output

together with the corresponding ECG. As we have already seen, the heart rhythm irregularity is common in both - ECG and PPG. Apart from that, the PPG during normal rhythm is more quasiperiodic when compared to the PPG during AF. We can see that this property is also transferred to the output of SSF - each successive peak is much more different in amplitude during AF when compared to the output during normal rhythm. Despite that, we can see that all peaks were detected correctly for both rhythms. The irregularity of the peak-to-peak intervals is much higher during AF than during normal rhythm, as expected. Please note that the scale of vertical axis for the row (e) is the same for both - Figure 3.1

and Figure 3.2 to make a decent comparison. The output of the algorithm is close to zero for normal rhythm signal and highly above threshold for AF signal. Therefore, the algorithm correctly identified both AF and normal rhythm signals in the presented examples.

Figure 3.3 shows the examples of the noise modeling for PPG signals at different SNR levels. The normal rhythm signals are displayed on the left side and the AF signals are displayed on the right side of the figure. The PPG without any noise is not displayed because it is visually indistinguishable from the PPG at the highest SNR level of 20 dB. The scale of the vertical axis is the same for all subplots for the sake of comparison. The PPG during atrial fibrillation appears to be smaller in amplitude than the PPG during normal rhythm, because of the scaling process. Since there are higher peaks present in the signal, the normalization process suppress the other parts of the signal. It is clear that at the noise levels down to 10 dB most of the peaks could still be detected. However, with the lower

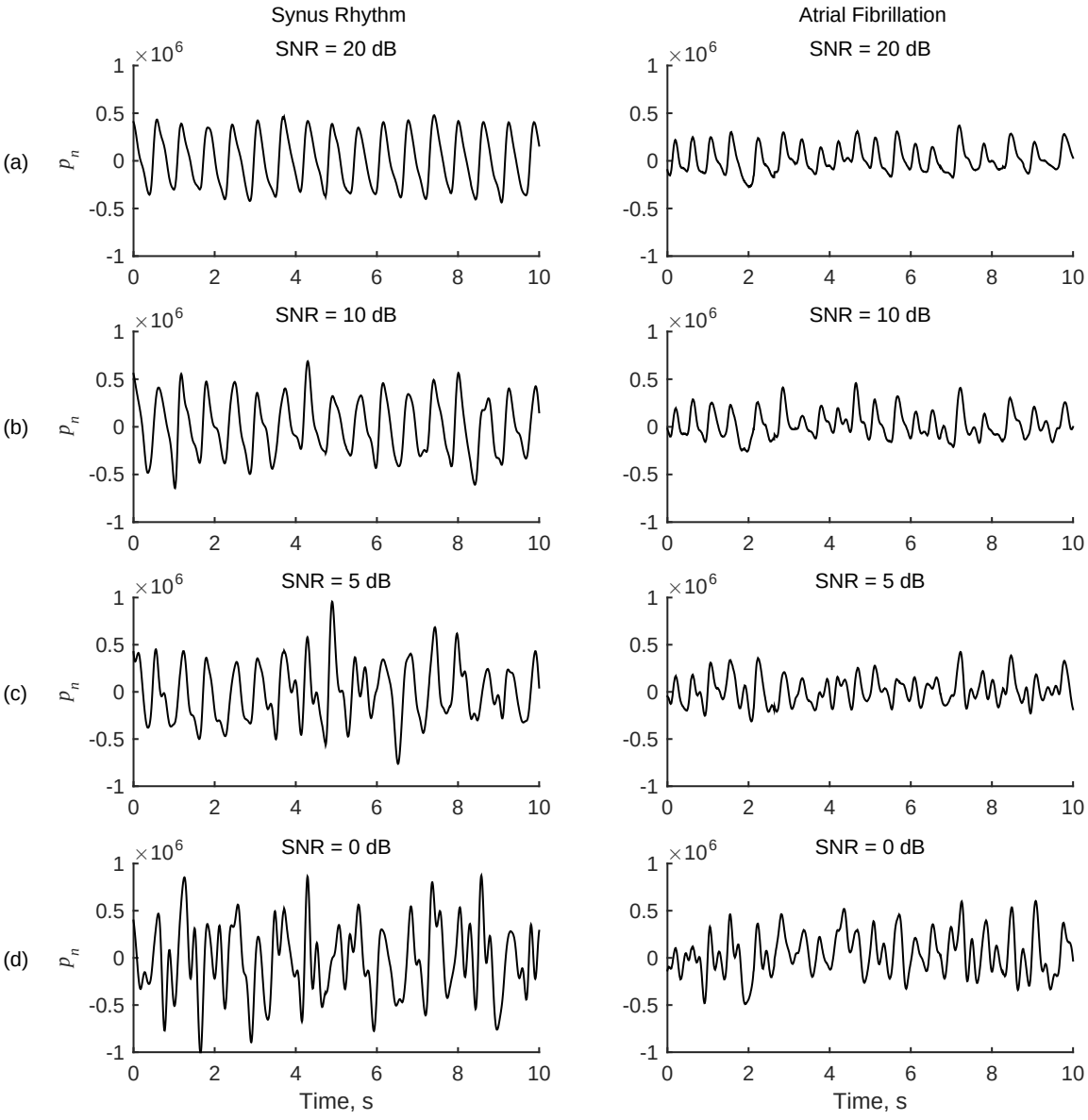


Figure 3.3: Examples of PPG with artificial noise at different SNR levels

SNR levels the noise becomes dominant and there is no possibility to distinguish between the peaks of the PPG pulses and the noise.

Examples with additional noise at 5 dB SNR for normal rhythm and AF are presented in Fig. 3.4 and Fig. 3.5, respectively. The first row of these figures displays the 20-bit scaled PPG which is the same PPG as in Figure 3.2 (b) and Figure 3.1 (b). The vertical scale for the rows (a) and (b) is the same for the sake of comparison. As we have already seen from the Figure 3.3, the PPG signals at the SNR level of 5 dB are already highly contaminated with the noise and the peaks of the PPG pulses become indistinguishable from the noise.

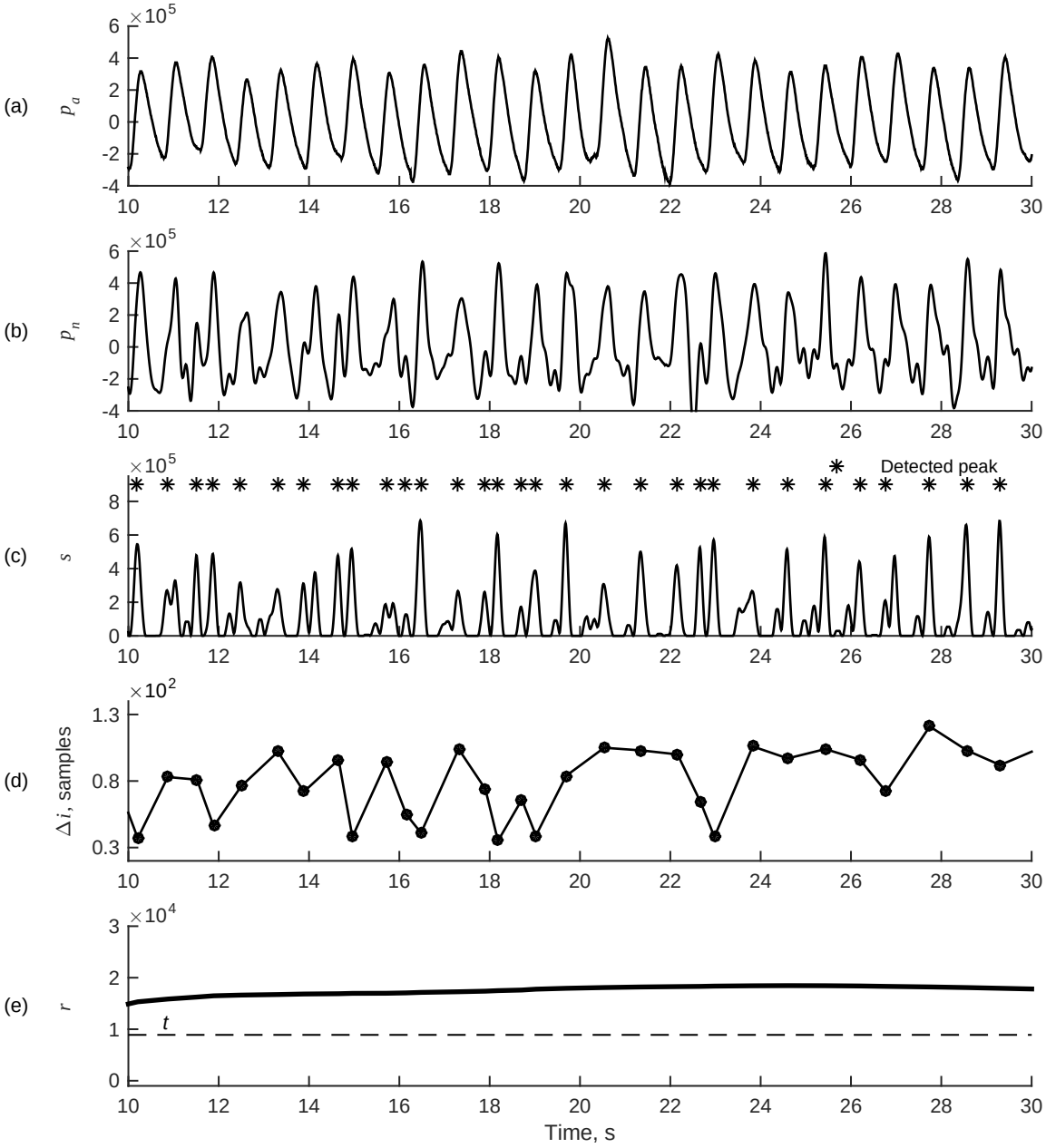


Figure 3.4: Processing of signals with normal rhythm at SNR level of 5 dB: (a) the PPG scaled to cover the 20-bit integer range, (b) the PPG with modeled noise, (c) the output of the SSF and the locations of the identified peaks, (d) the peak-to-peak intervals, (e) the continuous output of the algorithm and the threshold $t$ for the binary output

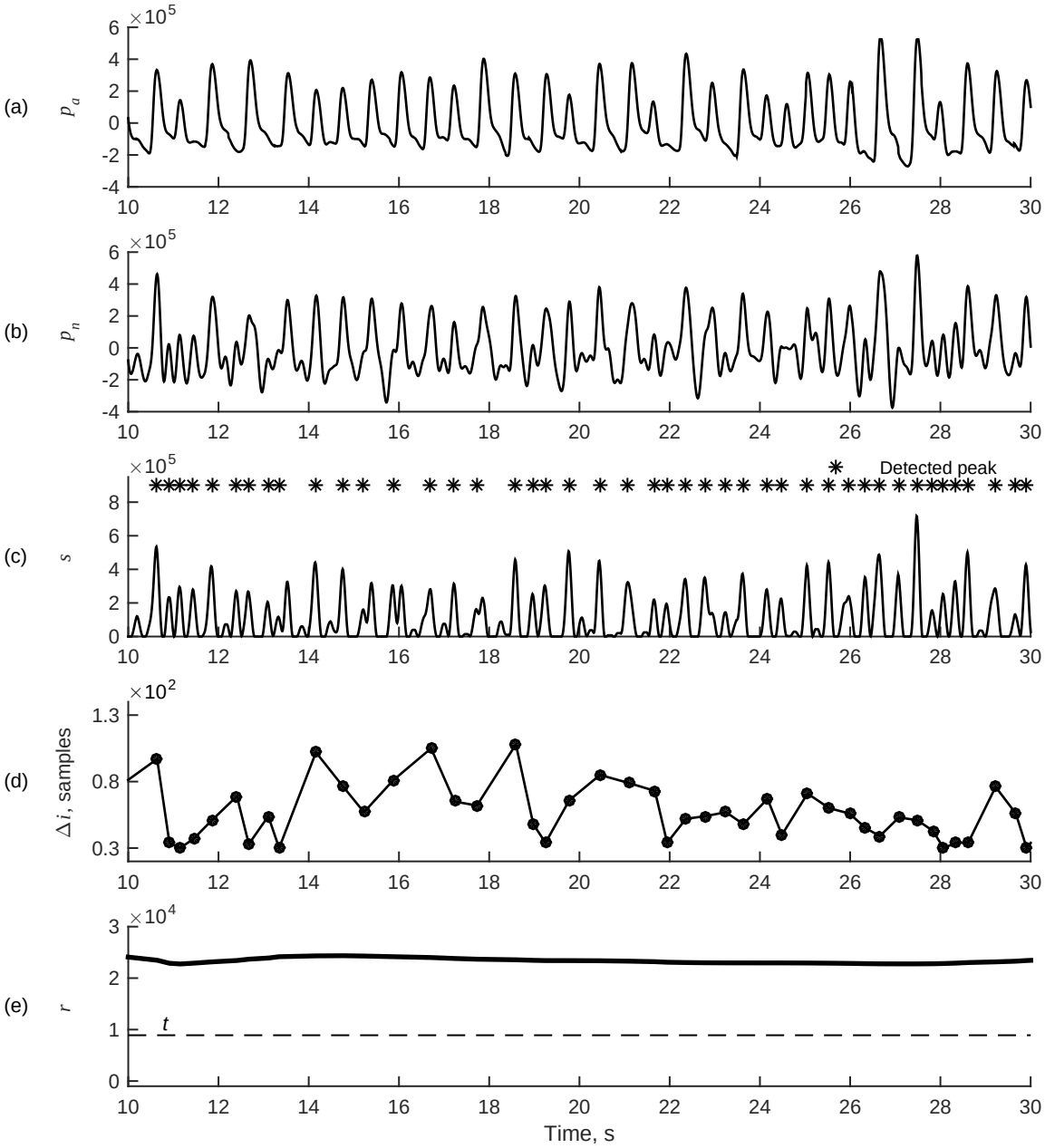


Figure 3.5: Processing of signals with AF at SNR level of 5 dB: (a) PPG scaled to cover the 20-bit integer range, (b) PPG with modeled noise, (c) output of SSF and locations of identified peaks, (d) peak-to-peak intervals, (e) continuous output of the algorithm and $t$ threshold for binary output

The same results can be seen in these examples. There are much more peaks in row (c) than it was originally in the PPG. Due to the stochastic origin of the noise, these peaks appear randomly and disturbs the peak-to-peak interval series. The noise shapes the interval series during the normal rhythm that it becomes more closer to that during AF. Therefore, we see that the algorithm incorrectly detects AF in the signal of normal rhythm. For the AF case, the continuous output of the algorithm is much higher above the threshold than at the SNR level of 20 dB.

## 3.2. Investigation of Algorithm's Performance

Figure 3.6 displays the sensitivity and specificity of the algorithm versus the threshold at different SNR levels. The point of 0.90 sensitivity is marked in rows (a) - (e). In the last row an additional point is marked, which is optimal at this specific case, since the specificity remains equal to 1 at even higher sensitivity than 0.90. Figure 3.7 displays the ROC curves at different SNR levels. We can see that the ROC curve for the SNR level of 0 dB is very

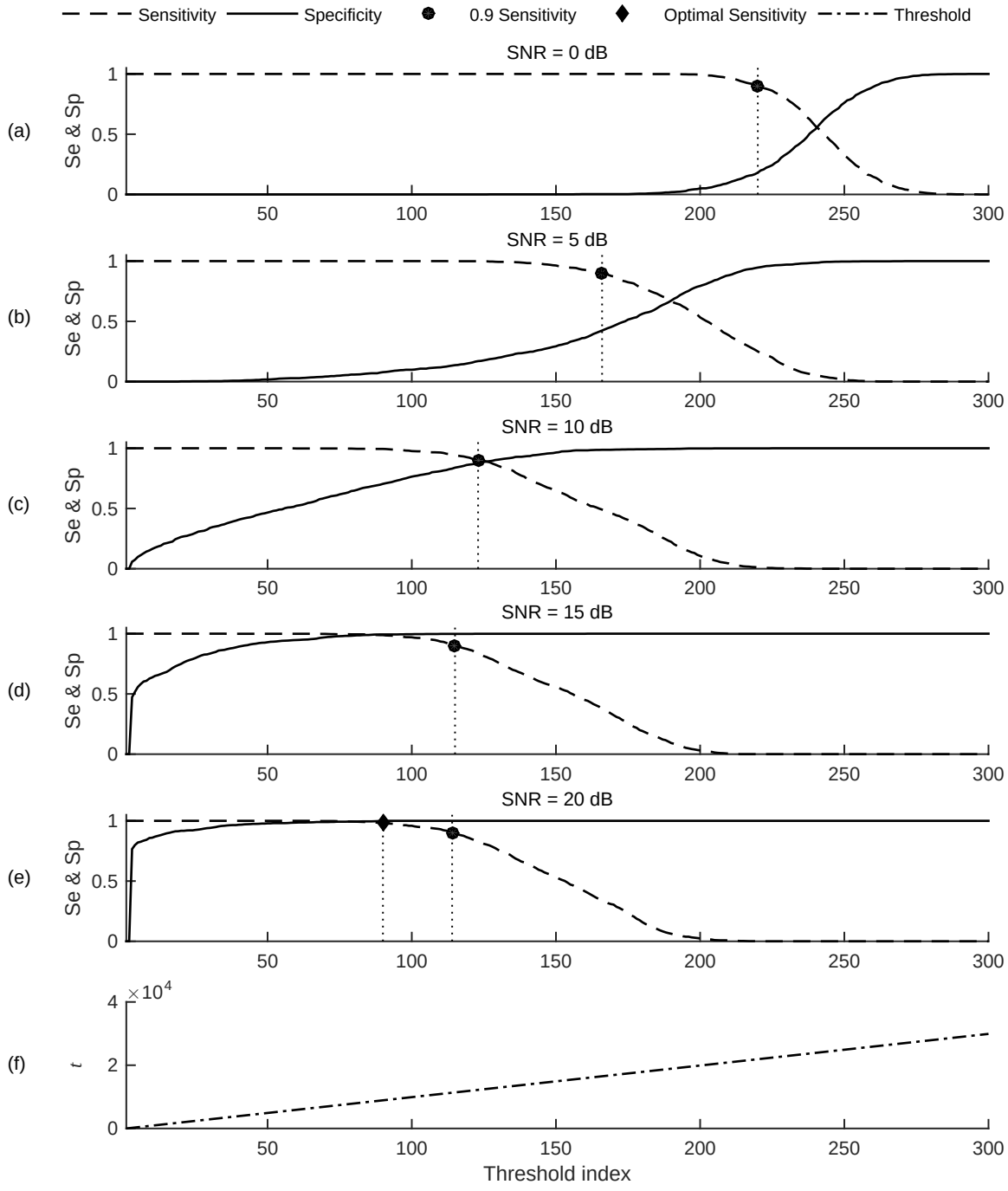


Figure 3.6: Sensitivity and specificity of the algorithm as a function of AF detection threshold at different SNR levels

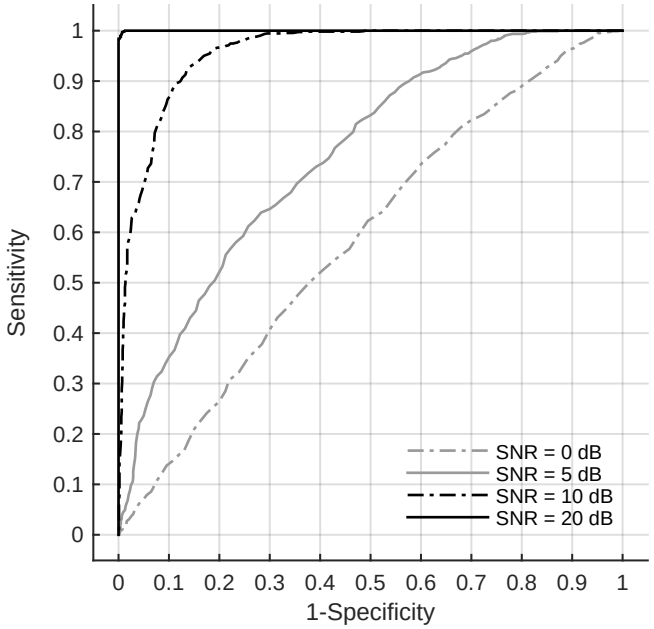


Figure 3.7: ROC curves at different SNR levels

close to the results of random guessing. While the ROC curve for the SNR level of 20 dB is close to the ROC curve of the ideal performance of a diagnostic test.

Figure 3.8 displays the area under the ROC curves for different SNR levels. We can see that the area holds close to linear relationship from the SNR level of 0 dB to 10 dB and the saturates to 0.99. The last three figures indicate that SNR levels down to 10 dB are manageable.

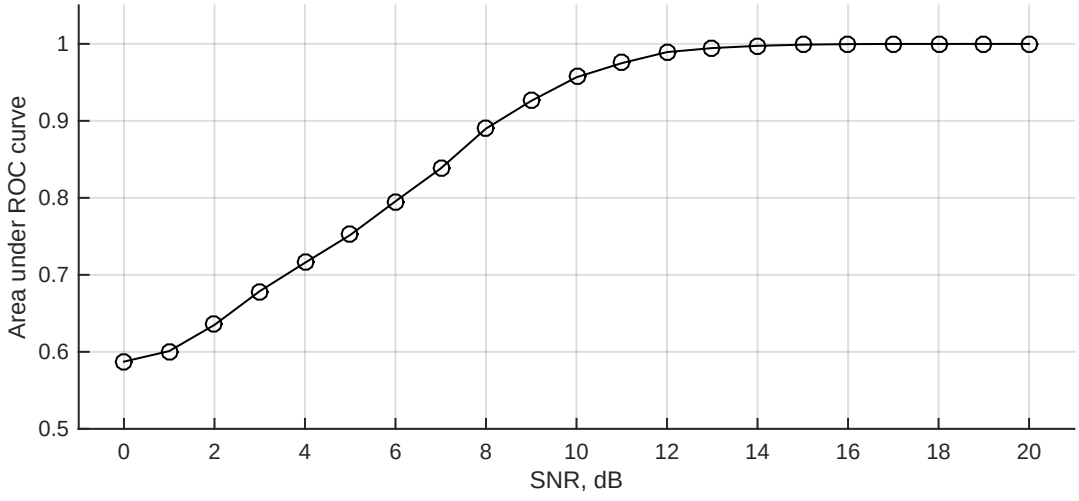


Figure 3.8: Area under ROC curve as a function of SNR

## 3.3. Investigation of Performance of Low-Quality-Signal Detector

Figure 3.9 shows the results of the algorithm for signal quality assessment. Histograms display the distribution of algorithm output for normal rhythm and atrial fibrillation at the

SNR levels of 20 dB when compared to 0 dB. As expected, the distinction between high-quality signal and artifacts is clearer for the normal rhythm than the AF. The output values for AF are between the values for normal rhythm and artifacts. We can see in Figure 3.9 (c) that the distinction between the high-quality signals and the motion artifacts is nearly perfect. Of course, with increasing SNR, the two histograms would end up closer to each other and the distinction would be not so clear. On the other hand, usually there are only two cases for the signal quality - either the quality is very high or very low. Therefore, such

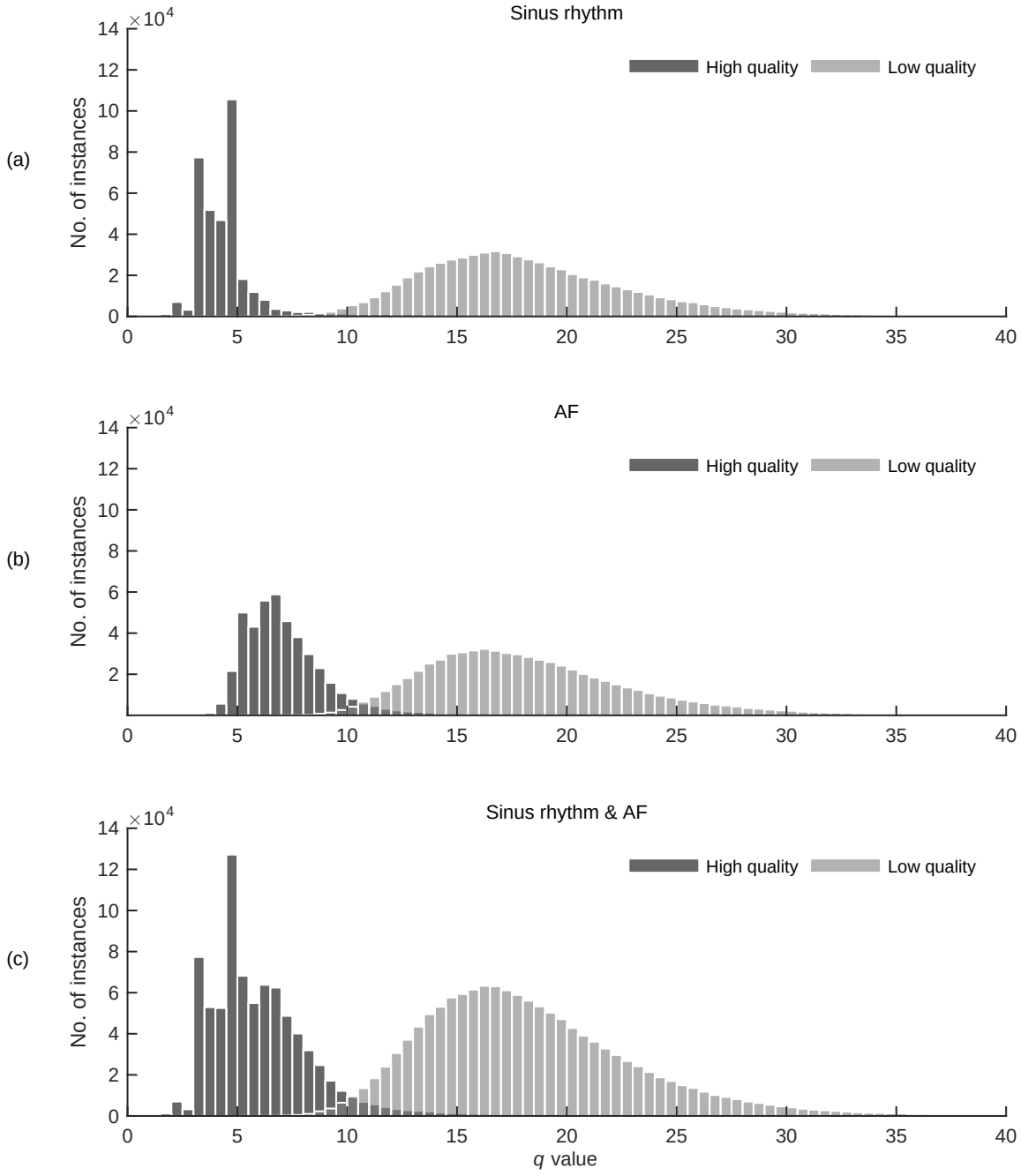


Figure 3.9: Histograms of output of the low-quality signal detector: (a) distribution of the output values for normal rhythm signals, (b) distribution of the output values for AF signals, (c) merged distributions for normal rhythm and AF signals

algorithm has a potential to be applied for distinction of PPG signal quality. The sensitivity and specificity of the low-quality-signal detection algorithm for the presented signal set with modeled noise is 0.99 and 0.90, respectively (see Fig. 3.10). Such high sensitivity was chosen in order to reduce false alarm rate. As we have already seen, the noise can be easily mistaken for signal during AF. Since AF is not a vitally important arrhythmia itself, a more conservative performance of the entire algorithm is desired.

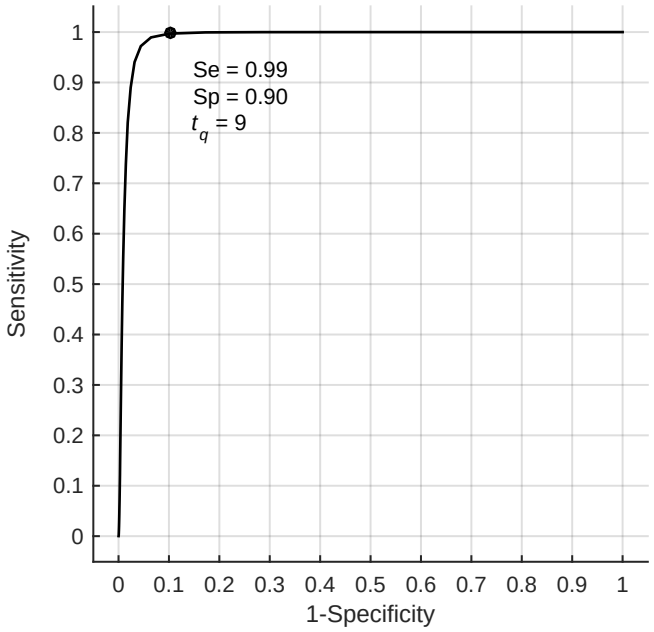


Figure 3.10: (a) PPG with high- and low-quality episodes, (b) output of the low-quality signal detector

Figure 3.11 shows an example from a ten-minute recording test. The high-quality region of a signal is marked at the beginning. We can see that the algorithm correctly identifies real motion artifacts. Although the output of the algorithm is highly varying and at several points the output decreases slightly below the threshold, the overall performance is acceptable. Please note that the threshold for low-quality-signal in Fig. 3.11 is already scaled according to Equation 2.43.

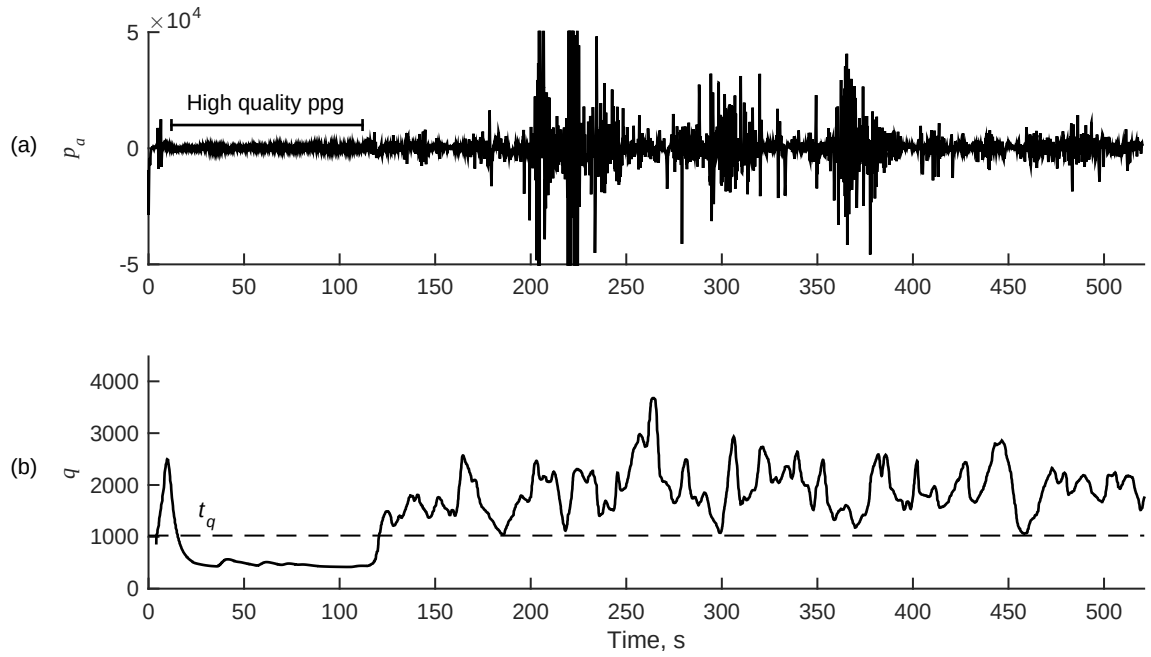


Figure 3.11: (a) PPG with high- and low-quality episodes, (b) output of the low-quality signal detector

## 3.4. Investigation of False Alarm Rate

Results from the one-hour-long recording test are presented in Table 3.1. The number and duration of false alarms, are presented as well as the duration of false alarms, corrected by low-quality-signal detector. We can see that in some cases the low-quality-signal detector significantly reduces the duration of false alarms, while in some cases does not affect the duration at all. It depends on the origin of false alarm - either it is motion artifact induced or induced due to high heart rate variability. The false alarm reduction due to the latter reason is out of the scope of this work. However, the presented results indicate that false alarms is a severe problem and should be addressed more extensively.

Table 3.1: Results from one-hour recording test

| Subject No. | No. of false alarms | Duration of false alarms, min | Corrected duration of false alarms, min |
|---|---|---|---|
| 1. | 25 | 14 | 14 |
| 2. | 20 | 13 | 13 |
| 3. | 20 | 25 | 17 |
| 4. | 24 | 40 | 28 |
| 5. | 10 | 53 | 45 |

## 3.5. Example of Algorithm's Performance in Embedded System

The algorithm was implemented in the presented embedded system and was capable of running in real time. The algorithm was implemented using integer arithmetic and scaled values presented earlier. The real-time operation was defined as processing each new sample of PPG during the pause between two successive sampling routines, which occur at rate of 250 Hz. Figure 3.12 shows the results calculated in the embedded system. This case was

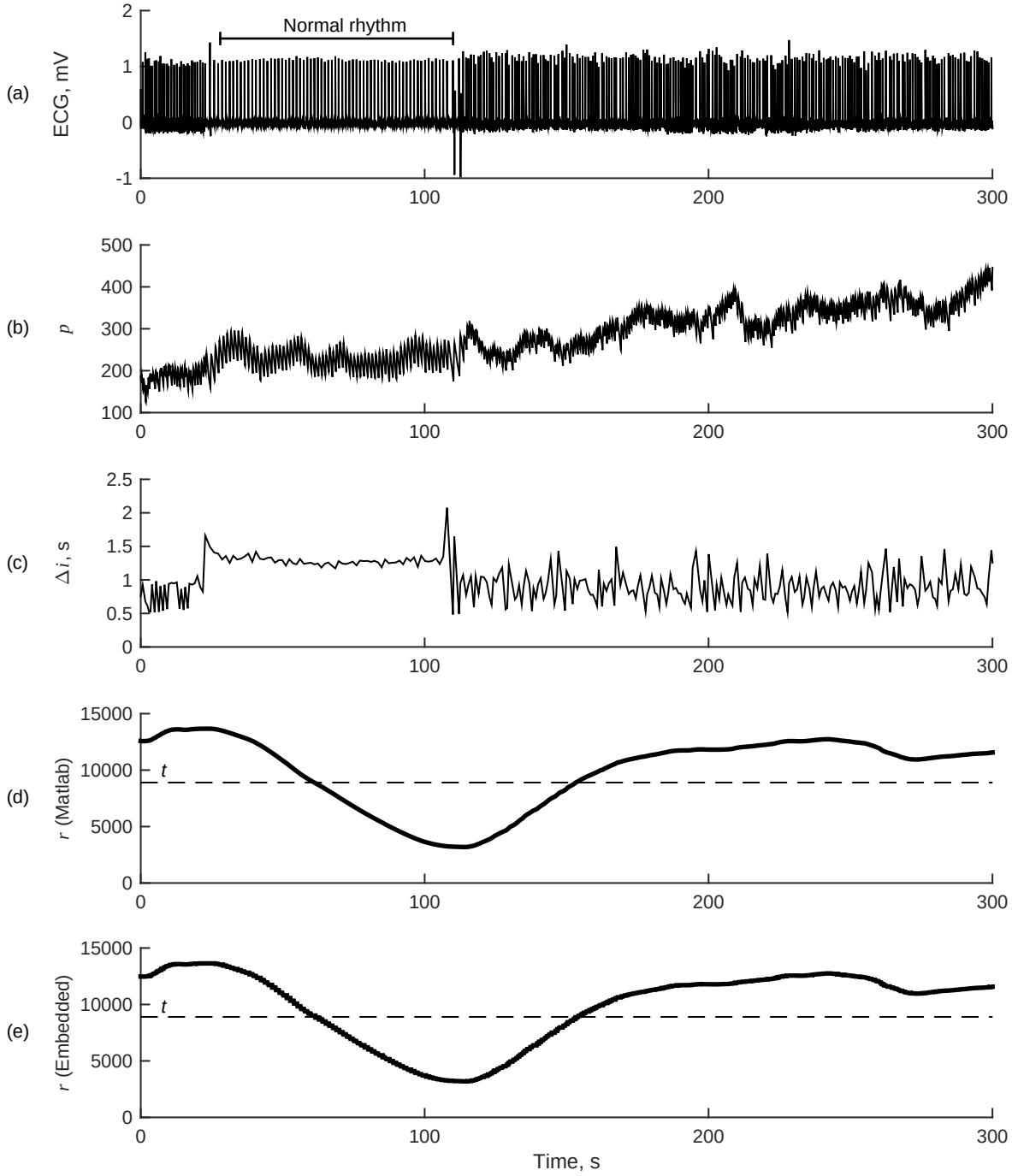


Figure 3.12: Results of the algorithm implemented in embedded system: (a) ECG and annotation, (b) unprocessed PPG, (c) RR interval series, (d) output of the algorithm in Matlab environtment, (e) output of the embedded system [48]

interesting, since the signal contains two episodes of AF and one episode of normal rhythm in between. Therefore, both transient processes are present - from normal rhythm to AF and vice versa. The delay in the output signals is present in the example - the output is not aligned to the input PPG. The results show that the both transitions between AF and normal rhythm were successfully detected by the algorithm in both versions - Matlab and embedded system. We can see that the output computed in embedded system is identical to that computed in Matlab. Therefore, we can state that the algorithm in embedded system performs adequately.

# Discussion

Assuming that RR intervals obtained from the ECG are equivalent to the peak-to-peak intervals of the PPG, any RR interval analysis based algorithm can be employed for decision making. The proposed system relies solely on heart rate properties, but morphology-based features could possibly be included as well. Figure 3.13 shows an example of false identification of AF signal as a normal rhythm signal due to slight variation of the output of the algorithm near the threshold. We can see that all peaks have been detected correctly, but

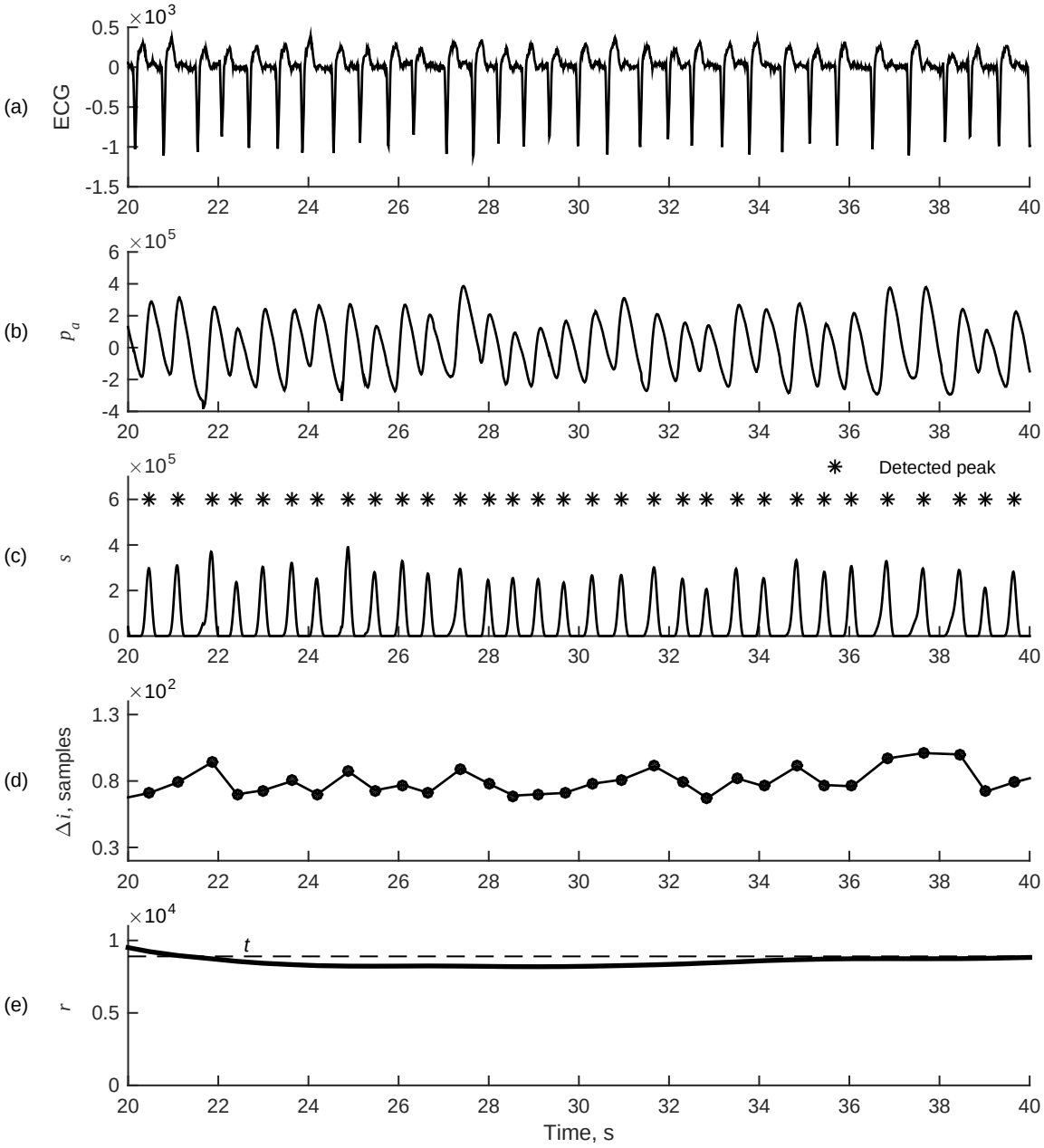


Figure 3.13: Incorrect outcome of the algorithm with AF signal: (a) ECG with removed baseline, (b) PPG scaled to cover the 20-bit integer range, (c) the output of the SSF and the locations of the detected peaks, (d) resulting peak-to-peak intervals, (e) the continuous output of the algorithm and the threshold for the binary output

the irregularity of heart rate is not high enough for AF to be detected. On the other hand, it is not clear if morphology-based features would help in such situation, since the morphology of the PPG is not very different from a PPG during normal rhythm.

Furthermore, it is crucial to detect PPG peaks correctly. Otherwise, falsely detected or undetected peaks may lead to false alarms, as we have already seen in Figure 3.4. In this study, we used a peak detector presented in [43]. However, this algorithm might require an improvement for peak detection during AF, since the adjacent peaks of the sum slope function may highly differ in amplitude compared to those observed during normal rhythm, as we have already seen in Figure 3.2.

Figure 3.14 shows an example of low-quality-signal detector performance when the high-quality signal is falsely identified as low-quality signal. We can see that the mistake occurs due to highly expressed dicrotic notch in PPG signal, which results in much higher variation of mean-cross count. Therefore, the output of the signal quality detection algorithm is slightly above the threshold. Such problem was absent during testing with records from MIMIC database, since the dicrotic notch was usually not present in these signals. A low-pass filter with lower cut-off frequency might be required to suppress the dicrotic notch in the PPG signal.

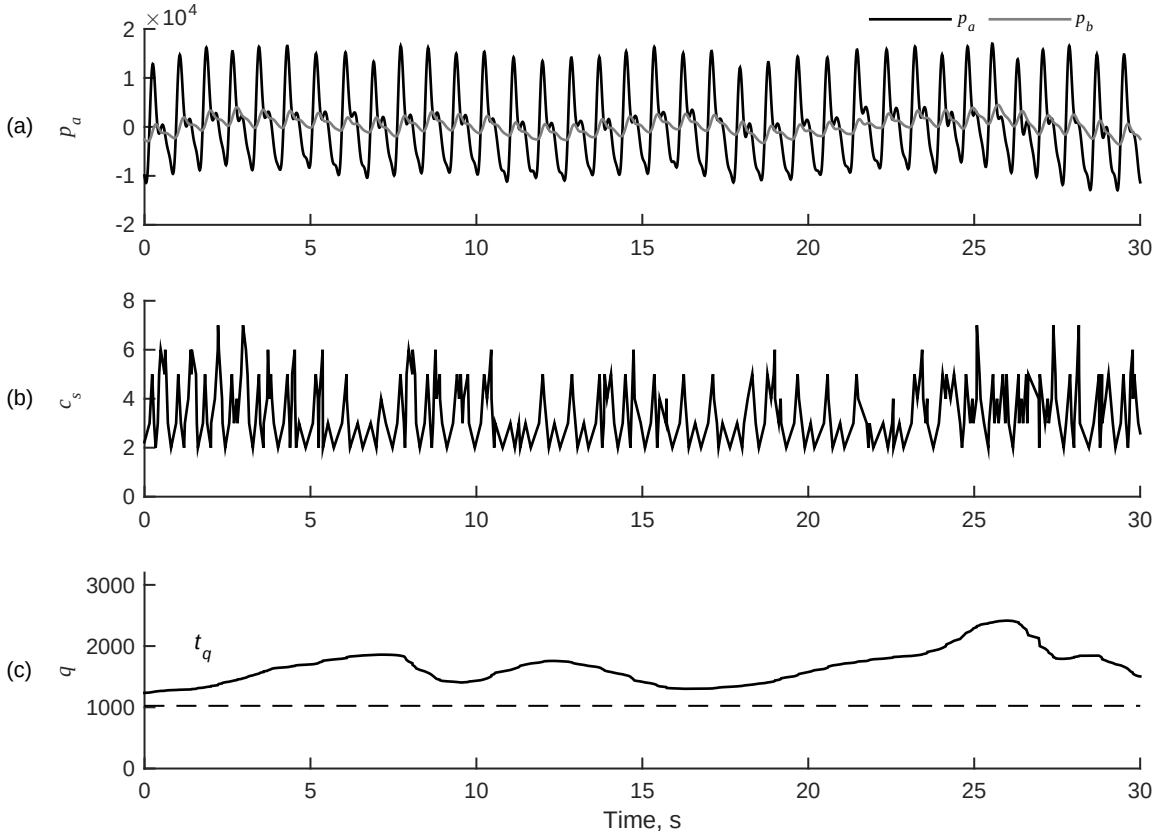


Figure 3.14: False detection of low-quality signal: (a) PPG with removed baseline and its time average, (b) mean-cross count, (c) output of the low-quality signal detector

Figure 3.15 shows another inadequate performance of the low quality signal detector. We can see that with increasing heart rate, the output of the algorithm increases as well. It happens due to sum component in the mean-cross count. Higher heart rate causes higher baseline for the mean-cross count signal and therefore, a higher sum of absolute values. In order to overcome this, baseline-independent value should be used instead of the running sum. Perhaps a standard deviation or first-derivative-based feature could be used instead.

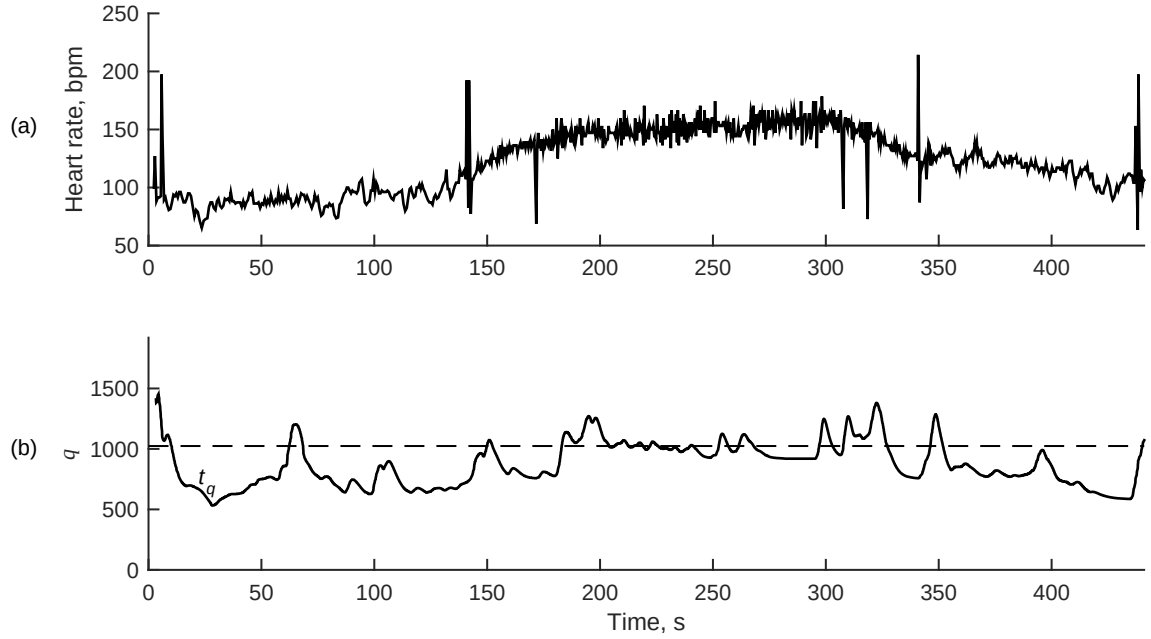


Figure 3.15: An example of false low-quality signal detection due elevated heart rate: (a) heart rate, (b) output of the low-quality signal detector

# Conclusions

The proposed algorithm embedded in a wearable device is suitable for an unobtrusive real-time AF detection using solely the PPG signal under low-activity condition.

The following objectives have been accomplished:

1. An algorithm for AF detection using solely the PPG signal has been developed. The building blocks of the proposed algorithm were designed to satisfy the requirement of low computational resources of a low-power embedded system.

2. An algorithm for low-quality PPG detection has been developed. The algorithm is suitable for distinction between high-quality signal and artifact-contaminated signal not only during normal rhythm, but during AF as well. When testing the performance with added noise, the algorithm showed sensitivity of 0.99 and specificity of 0.90.

3. The algorithm has been implemented in a low-power embedded system to be running in real-time. While sampling PPG at 250 samples per second, the ARM Cortex-M0 core running at 16 MHz is capable of processing each sample in between the sampling routines.

4. A set of synchronous PPG and ECG signals has been collected from the public MIMIC database. When testing the performance with noise-free signals the algorithm showed sensitivity of 0.96 and perfect specificity of 1.

# References


1. ZEBE, H. Atrial fibrillation in dialysis patients. *Nephrology Dialysis Transplantation*, n. 6, p. 765–768, jun. ISSN 1460-2385.

2. GUSSAK, I.; GUSSAK, H. M. Sudden cardiac death in nephrology: focus on acquired long QT syndrome. *Nephrology Dialysis Transplantation*, n. 1, p. 12–14, oct. ISSN 0931-0509.

3. MAINARDI, L.; SÖRNMO, L.; CERUTTI, S. *Understanding Atrial Fibrillation: The Signal Processing Contribution, Part I*: Morgan & Claypool Publishers, 2008. vol. 3. 1–129 p. ISSN 1930-0336. ISBN 9-781-598-29297-8.

4. CHUGH, S. S. et al. Worldwide Epidemiology of Atrial Fibrillation: A Global Burden of Disease 2010 Study. *Circulation*, n. 8, p. 837–847, feb. ISSN 0009-7322.

5. JANUARY, C. T. et al. 2014 AHA/ACC/HRS Guideline for the Management of Patients With Atrial Fibrillation. *Journal of the American College of Cardiology*, n. 21, p. e1–e76, dec. ISSN 0735-1097.

6. ABBOTT, K. C. et al. Atrial fibrillation in chronic dialysis patients in the United States: risk factors for hospitalization and mortality. *BMC Nephrol*, n. 1, p. 1. ISSN 1471-2369.

7. LEE, J. et al. Atrial fibrillation detection using an iphone 4S. *IEEE Transactions on Biomedical Engineering*, vol. 60, n. 1, p. 203–206, 2013. ISSN 0018-9294.

8. PETRĖNAS, A. *Detection of Brief Episode Paroxysmal Atrial Fibrillation*. Thesis (Doctoral) — Kaunas University of Technology, 2015.

9. GOLDBERGER, A. L. *Clinical Electrocardiography: A Simplified Approach*: Elsevier. ISBN 978-0-323-04038-9.

10. MAROZAS, V.; JEGELEVIČIUS, D. *Biomedicininių signalų skaitmeninis apdorojimas*: Nomparelis, 2008.

11. KANIUSAS, E. *Biomedical Signals and Sensors II - Linking Acoustic and Optic Biosignals and Biomedical Sensors*: Springer-Verlag Berlin Heidelberg. ISBN 978-3-662-45106-9.

12. ELGENDI, M. On the analysis of fingertip photoplethysmogram signals. *Current cardiology reviews*, vol. 8, n. 1, p. 14–25, 2012. ISSN 1875-6557.

13. CLARK, D. M. et al. Hemodynamic effects of an irregular sequence of ventricular cycle lengths during atrial fibrillation. *Journal of the American College of Cardiology*, n. 4, p. 1039–45, oct. ISSN 0735-1097.

14. LIP, G. Y. H. et al. Prognosis and treatment of atrial fibrillation patients by European cardiologists: One Year Follow-up of the EURObservational Research Programme-Atrial Fibrillation General Registry Pilot Phase (EORP-AF Pilot registry). *European Heart Journal*, n. 47, p. 3365–3376, dec. ISSN 0195-668X.

15. GAILLARD, N. et al. Detection of paroxysmal atrial fibrillation with transtelephonic EKG in TIA or stroke patients. *Neurology*, n. 21, p. 1666–1670, may. ISSN 0028-3878.

16. HEALEY, J. S. et al. Subclinical Atrial Fibrillation and the Risk of Stroke. *New England Journal of Medicine*, Massachusetts Medical Society, n. 2, p. 120–129, jan. ISSN 0028-4793.

17. LOWRES, N. et al. Screening to identify unknown atrial fibrillation. *Thrombosis and Haemostasis*, n. 2, p. 213–222, apr. ISSN 0340-6245.

18. CAMM, A. J. et al. Guidelines for the management of atrial fibrillation: The Task Force for the Management of Atrial Fibrillation of the European Society of Cardiology (ESC). *European Heart Journal*, n. 19, p. 2369–2429, oct. ISSN 0195-668X.

19. LAMORI, J. C. et al. Burden of comorbidities among patients with atrial fibrillation. *Therapeutic Advances in Cardiovascular Disease*, n. 2, p. 53–62, apr. ISSN 1753-9447.

20. MARINI, C. et al. Contribution of Atrial Fibrillation to Incidence and Outcome of Ischemic Stroke: Results From a Population-Based Study. *Stroke*, n. 6, p. 1115–1119, jun. ISSN 0039-2499.

21. LAGUNA, P.; JANE, R.; CAMINAL, P. Adaptive filtering of ECG baseline wander. In: *Proceedings of the Annual International Conference of the IEEE Engineering in Medicine and Biology Society*: IEEE. p. 508–509. ISBN 0-7803-0785-2.

22. *Kidney Failure: Choosing a Treatment That's Right for You.* http://www.niddk.nih.gov/health-information/health-topics/kidney-disease/kidney-failure-choosing-a-treatment-thats-right-for-you/Pages/facts.aspx. Last accessed: 2015-06-24.

23. GOLDSTEIN, B. a. et al. Trends in the incidence of atrial fibrillation in older patients initiating dialysis in the United States. *Circulation*, vol. 126, n. 19, p. 2293–2301, 2012. ISSN 0009-7322.

24. WINKELMAYER, W. C. et al. The increasing prevalence of atrial fibrillation among hemodialysis patients. *Journal of the American Society of Nephrology : JASN*, vol. 22, n. 2, p. 349–357, 2011. ISSN 1533-3450.

25. *Study the Characteristics of Cardiac Related Events in Hemodialysis Patients (MiD).* https://clinicaltrials.gov/ct2/show/study/NCT01779856. Last accessed: 2015-06-24.

26. COSTEA, A. I. et al. Abstract 19584: Frequency and Distribution of Hemodialysis (HD)-Associated Atrial Fibrillation: Preliminary Results of the (MiD) Study. *Circulation*, n. Suppl_2, p. A19584–, nov.

27. *Medtronic Study Reveals Significant Heart Rhythm Disorders Occurring in Patients Undergoing Hemodialysis.* http://newsroom.medtronic.com/phoenix.zhtml?c=251324&p=irol-newsArticle&ID=1989694. Last accessed: 2015-06-24.

28. DASH, S. et al. Automatic real time detection of atrial fibrillation. *Annals of biomedical engineering*, n. 9, p. 1701–9, sep. ISSN 1573-9686.

29. HUANG, C. et al. A novel method for detection of the transition between atrial fibrillation and sinus rhythm. *IEEE transactions on bio-medical engineering*, n. 4, p. 1113–9, apr. ISSN 1558-2531.

30. BABAEIZADEH, S. et al. Improvements in atrial fibrillation detection for real-time monitoring. *Journal of electrocardiology*, n. 6, p. 522–6, jan. ISSN 1532-8430.

31. GACEK, A.; PEDRYCZ, W. (Ed.). *ECG Signal Processing, Classification and Interpretation*. London: Springer London. ISBN 978-0-85729-867-6.

32. PETRĖNAS, A.; MAROZAS, V.; SÖRNMO, L. Low-complexity detection of atrial fibrillation in continuous long-term monitoring. *Computers in biology and medicine*, jan. ISSN 1879-0534.

33. ASGARI, S.; MEHRNIA, A.; MOUSSAVI, M. Automatic detection of atrial fibrillation using stationary wavelet transform and support vector machine. *Computers in Biology and Medicine*, Elsevier, p. 132–142. ISSN 0010-4825.

34. LI, K.; WARREN, S.; NATARAJAN, B. Onboard Tagging for Real-Time Quality Assessment of Photoplethysmograms Acquired by a Wireless Reflectance Pulse Oximeter. *IEEE Transactions on Biomedical Circuits and Systems*, n. 1, p. 54–63, feb. ISSN 1932-4545.

35. ORPHANIDOU, C. et al. Signal Quality Indices for the Electrocardiogram and Photoplethysmogram: Derivation and Applications to Wireless Monitoring. *IEEE Journal of Biomedical and Health Informatics*, n. 3, p. 1–1. ISSN 2168-2194.

36. LI, Q.; CLIFFORD, G. D. Dynamic time warping and machine learning for signal quality assessment of pulsatile signals. *Physiological Measurement*, n. 9, p. 1491–1501, sep. ISSN 0967-3334.

37. ANDERSSON, O. et al. A 290 mV Sub- VT ASIC for Real-Time Atrial Fibrillation Detection. *IEEE transactions on biomedical circuits and systems*, out. ISSN 1940-9990.

38. MOODY, G. B.; MARK, R. G. The impact of the MIT-BIH arrhythmia database. *IEEE engineering in medicine and biology magazine : the quarterly magazine of the Engineering in Medicine & Biology Society*, n. 3, p. 45–50, jan. ISSN 0739-5175.

39. PETRUTIU, S.; SAHAKIAN, A. V.; SWIRYN, S. Abrupt changes in fibrillatory wave characteristics at the termination of paroxysmal atrial fibrillation in humans. *Europace : European pacing, arrhythmias, and cardiac electrophysiology : journal of the working groups on cardiac pacing, arrhythmias, and cardiac cellular electrophysiology of the European Society of Cardiology*, n. 7, p. 466–70, jul. ISSN 1099-5129.

40. MOODY, G.; MARK, R. A database to support development and evaluation of intelligent intensive care monitoring. In: *Computers in Cardiology 1996*: IEEE. p. 657–660. ISBN 0-7803-3710-7. ISSN 0276-6547.

41. SAEED, M. et al. Multiparameter Intelligent Monitoring in Intensive Care II: a public-access intensive care unit database. *Critical care medicine*, vol. 39, n. 5, p. 952–60, 2011. ISSN 1530-0293.

42. *A Simple Software Lowpass Filter Suits Embedded-System Applications.* http://www.edn.com/design/systems-design/4320010/A-simple-software-lowpass-filter-suits-embedded-system-applications. Last accessed: 2016-05-23.

43. JANG, D.-G. et al. A Real-Time Pulse Peak Detection Algorithm for the Photoplethysmogram. *International Journal of Electronics and Electrical Engineering*, n. 1, p. 45–49. ISSN 2301-380X.

44. JALIL, M.; BUTT, F. A.; MALIK, A. Short-time energy, magnitude, zero crossing rate and autocorrelation measurement for discriminating voiced and unvoiced segments of speech signals. In: *2013 The International Conference on Technological Advances in Electrical, Electronics and Computer Engineering (TAEECE)*: IEEE. p. 208–212. ISBN 978-1-4673-5613-8.

45. GOLDBERGER, A. L. et al. PhysioBank, PhysioToolkit, and PhysioNet : Components of a New Research Resource for Complex Physiologic Signals. *Circulation*, n. 23, p. e215–e220, jun. ISSN 0009-7322.

46. GARGASAS, L. et al. Functional State Evaluation System with Distributed Intellect for Elderly and Disabled Persons. *Technologies of Computer Control*, vol. 13, p. 57–62, 2012.

47. STANKEVIČIUS, D.; MAROZAS, V. Multisensory Wristwatch System for Unobtrusive Physiological and Kinematical Signals Recording. In: *Biomedical Engineering 2014*, 2014. vol. 18, p. 162–167.

48. STANKEVIČIUS, D. et al. Photoplethysmography-Based System for Atrial Fibrillation Detection During Hemodialysis. In: : Springer International Publishing, (IFMBE Proceedings). p. 79–82. ISBN 978-3-319-32701-3.

# Appendices

## Appendix No. 1. Details of the Records from MIMIC Database

| No. | Record Name | Type | Age | Sex | No. of Signals |
|---|---|---|---|---|---|
| 1 | 208m | AF | 80 | M | 40 |
| 2 | 209m | | | | 164 |
| 3 | 210m | | | | 227 |
| 4 | 231m | | 75 | F | 29 |
| 5 | 248m | | 80 | F | 20 |
| 6 | 276m | | 66 | F | 96 |
| 7 | 430m | | 91 | M | 123 |
| 8 | 438m | | 78 | M | 117 |
| 9 | 442m | | 67 | F | 92 |
| 10 | 452m | | 73 | M | 80 |
| 11 | 471m | | 78 | F | 34 |
| 12 | 472m | | 79 | M | 83 |
| 13 | 041m | Normal rhythm | 70 | M | 43 |
| 14 | 055m | | 38 | M | 12 |
| 15 | 211m | | 67 | F | 12 |
| 16 | 212m | | 84 | M | 61 |
| 17 | 213m | | 82 | F | 38 |
| 18 | 218m | | 67 | M | 40 |
| 19 | 219m | | | | 33 |
| 20 | 220m | | 68 | F | 13 |
| 21 | 221m | | | | 52 |
| 22 | 224m | | 21 | M | 51 |
| 23 | 225m | | 73 | M | 61 |
| 24 | 226m | | 68 | M | 84 |
| 25 | 230m | | 75 | F | 44 |
| 26 | 231m | | | | 15 |
| 27 | 237m | | 63 | F | 21 |
| 28 | 240m | | 68 | M | 16 |

| No. | Record Name | Type | Age | Sex | No. of Signals |
|---|---|---|---|---|---|
| 29 | 252m | Normal rhythm | 52 | M | 15 |
| 30 | 253m | | | | 15 |
| 31 | 254m | | | | 25 |
| 32 | 260m | | 76 | F | 24 |
| 33 | 276m | | 66 | F | 30 |
| 34 | 281m | | 61 | M | 45 |
| 35 | 284m | | 59 | F | 41 |
| 36 | 401m | | 64 | F | 36 |
| 37 | 403m | | | | 60 |
| 38 | 404m | | 87 | F | 5 |
| 39 | 410m | | 57 | M | 74 |
| 40 | 411m | | 82 | F | 80 |
| 41 | 414m | | 92 | F | 1 |
| 42 | 427m | | 48 | M | 53 |

## Appendix No. 2. List of Dissemination Activities

Some of the results of this thesis have been or will be presented in the following events:

- XIV Mediterranean Conference on Medical and Biological Engineering and Computing (Paphos, Cyprus, 2016). The publication:

  STANKEVIČIUS, D.; PETRĖNAS, A.; SOLOŠENKO, A; GRIGUTIS, M.; JANUŠKEVIČIUS, T.; RIMŠEVIČIUS, L.; and MAROZAS, V.
  Photoplethysmography-Based System for Atrial Fibrillation Detection During Hemodialysis. In Springer International Publishing, (IFMBE Proceedings, vol. 57), p. 79-82. ISBN 9783319327013.

- The 15th Biennial Conference on Electronics and Embedded Systems (Tallin, Estonia, 2016). The publication:

  STANKEVIČIUS, D.; PETRĖNAS, A.; SOLOŠENKO, A; MICKUS, T.; DAUKANTAS, S; MAROZAS, V.; KUŠLEIKAITĖ, N.; SKIBARKIENĖ, J.; KUBILIUS, R.; and BUMBLYTĖ, I.
  Unobtrusive Device for Paroxysmal Atrial Fibrillation Detectin under Low-Activity Conditions. *Under review.*

- International exhibition / competition „Technorama 2015“ (Kaunas, Lithuania, 2015). The presentation:

  SOLOŠENKO, A; STANKEVIČIUS, D.; PETRĖNAS, A.; MAROZAS, V.; GRIGUTIS, M.; JANUŠKEVIČIUS, T.; and RIMŠEVIČIUS, L.
  Real-Time System for Atrial Fibrillation Detection During Hemodialysis.

- International exhibition / competition „Technorama 2016“ (Kaunas, Lithuania, 2016). The presentation:

  STANKEVIČIUS, D.; SOLOŠENKO, A; MICKUS, T.; PETRĖNAS, A.; DAUKANTAS, S; MAROZAS, V.; SKIBARKIENĖ, J.; and KUBILIUS, R.
  Unobtrusive Long-Term Monitoring System for Myocardial Infarction Induced Atrial Fibrillation Detection.